





Review

Diagnosis of Glioblastoma by Immuno-Positron Emission Tomography

Eduardo Ruiz-López ¹, Juan Calatayud-Pérez ², Irene Castells-Yus ¹, María José Gimeno-Peribáñez ³, Noelia Mendoza-Calvo ¹, Miguel Ángel Morcillo ^{4,*} and Alberto J. Schuhmacher ^{1,5,*}

¹ Molecular Oncology Group, Instituto de Investigación Sanitaria Aragón (IIS Aragón), 50009 Zaragoza, Spain; eruiz@iisaragon.es (E.R.-L.); icastells@iisaragon.es (I.C.-Y.); nmendoza@iisaragon.es (N.M.-C.)

² Department of Neurosurgery, Lozano Blesa University Clinical Hospital, 50009 Zaragoza, Spain; jbcalatayud@salud.aragon.es

³ Department of Radiology, Lozano Blesa University Clinical Hospital, 50009 Zaragoza, Spain; mjgimeno@comz.org

⁴ Biomedical Application of Radioisotopes and Pharmacokinetics Unit, Centro de Investigaciones Energéticas, Medioambientales y Tecnológicas (CIEMAT), 28040 Madrid, Spain

⁵ Fundación Agencia Aragonesa Para la Investigación y el Desarrollo (ARAID), 50018 Zaragoza, Spain

* Correspondence: mangel.morcillo@ciemat.es (M.Á.M.); ajimenez@iisaragon.es (A.J.S.)

Simple Summary: Neuroimaging has transformed the way brain tumors are diagnosed and treated. Although different non-invasive modalities provide very helpful information, in some situations, they present a limited value. By merging the specificity of antibodies with the resolution, sensitivity, and quantitative capabilities of positron emission tomography (PET), “Immuno-PET” allows us to conduct the non-invasive diagnosis and monitoring of patients over time using antibody-based probes as an in vivo, integrated, quantifiable, 3D, full-body “immunohistochemistry”, like a “virtual biopsy”. This review provides and focuses on immuno-PET applications and future perspectives of this promising imaging approach for glioblastoma.



Citation: Ruiz-López, E.; Calatayud-Pérez, J.; Castells-Yus, I.; Gimeno-Peribáñez, M.J.; Mendoza-Calvo, N.; Morcillo, M.Á.; Schuhmacher, A.J. Diagnosis of Glioblastoma by Immuno-Positron Emission Tomography. *Cancers* **2022**, *14*, 74. <https://doi.org/10.3390/cancers14010074>

Academic Editor: Jorn Fierstra

Received: 24 November 2021

Accepted: 21 December 2021

Published: 24 December 2021

Publisher’s Note: MDPI stays neutral with regard to jurisdictional claims in published maps and institutional affiliations.



Copyright: © 2021 by the authors. Licensee MDPI, Basel, Switzerland. This article is an open access article distributed under the terms and conditions of the Creative Commons Attribution (CC BY) license (<https://creativecommons.org/licenses/by/4.0/>).

Abstract: Neuroimaging has transformed neuro-oncology and the way that glioblastoma is diagnosed and treated. Magnetic Resonance Imaging (MRI) is the most widely used non-invasive technique in the primary diagnosis of glioblastoma. Although MRI provides very powerful anatomical information, it has proven to be of limited value for diagnosing glioblastomas in some situations. The final diagnosis requires a brain biopsy that may not depict the high intratumoral heterogeneity present in this tumor type. The revolution in “cancer-omics” is transforming the molecular classification of gliomas. However, many of the clinically relevant alterations revealed by these studies have not yet been integrated into the clinical management of patients, in part due to the lack of non-invasive biomarker-based imaging tools. An innovative option for biomarker identification in vivo is termed “immunotargeted imaging”. By merging the high target specificity of antibodies with the high spatial resolution, sensitivity, and quantitative capabilities of positron emission tomography (PET), “Immuno-PET” allows us to conduct the non-invasive diagnosis and monitoring of patients over time using antibody-based probes as an in vivo, integrated, quantifiable, 3D, full-body “immunohistochemistry” in patients. This review provides the state of the art of immuno-PET applications and future perspectives on this imaging approach for glioblastoma.

Keywords: diagnostic imaging; immuno-PET; glioblastoma; neuroimaging; molecular imaging; antibody; nanobody; theragnostic probes

1. Introduction

Glioblastoma is the most common and aggressive tumor of the central nervous system in adults [1]. With an incidence of 3.23 cases per 100,000 individuals in Europe and the USA, glioblastoma represents ~49.1% of primary malignant brain tumors [1,2]. Despite continuous advances in the molecular classification of glioblastoma, and the steady progress

in surgical, radiological, and chemotherapeutic treatment options [1,3,4], patient survival has improved only marginally during the past 3 decades. Current glioblastoma survival rates average just 8–14.6 months, with only ~5% of patients surviving more than 5 years [1,5]. Recurrence of glioblastoma is nearly universal and is associated with poor prognosis; patients with recurrent glioblastoma have a median survival of only 5–7 months with optimal therapy [6].

The current standard-of-care for treatment of newly diagnosed glioblastoma has remained relatively unchanged since 2005 and consists of maximal safe resection followed by concomitant chemoradiation with the alkylating agent temozolomide (TMZ), and subsequent adjuvant TMZ [7].

The DNA-repair enzyme O⁶-methylguanine-DNA methyltransferase (MGMT) impairs the killing of tumor cells by alkylating agents chemotherapy [8]. Methylation of the *MGMT* promoter regulates its expression. Despite confirming the prognostic significance of *MGMT* promoter methylation, survival did not improve with TMZ [9].

In 2011, a novel therapeutic approach, the first-generation tumor treating fields (TTF) device, was approved by the Food and Drug Administration (FDA) for the treatment of recurrent glioblastoma [10]. The TTF device was subsequently approved as adjuvant therapy for newly-diagnosed glioblastoma in 2015 [10,11].

Resistance to current treatments involves a complex interplay of numerous molecular mechanisms. Advances in the molecular classification of glioblastomas will likely translate into the development of novel and more effective therapeutic approaches that will improve glioblastoma patient outcomes.

2. Current Status of Glioblastoma Classification and Diagnosis

The 2016 World Health Organization (WHO) Classification of Tumors of the Central Nervous System (WHO CNS4) incorporated for the first time genetic alterations into the classification system to create more homogenous disease categories with greater prognostic value [12]. The WHO CNS4 classification symbolized a paradigm shift, replacing classical histology-based glioma diagnostics with an integrated histological and molecular classification system that enables more precise tumor categorization [12,13]. The incorporated diagnostic biomarkers in the 2016 WHO classification of gliomas were Isocitrate dehydrogenase (*IDH*)-1/2 mutations, 1p/19q codeletion, H3 Histone, Family 3A (*H3F3A*) or HIST1H3B/C K27M (*H3-K27M*) mutations, and *C11orf95-RELA* fusions [13].

The novel 2021 classification (WHO CNS5) moves further to advance the role of molecular diagnostics in CNS tumor classification but still remains rooted in other established approaches to tumor characterization, including histology and immunohistochemistry [14]. The WHO CNS5 assumes that most tumor types are aligned to distinct methylation profiles [15]. While these are not specified in every tumor definition, the information about diagnostic methylation is included in the “Definitions” and “Essential and Desirable Diagnostic Criteria” sections of WHO CNS5 and could provide more critical guidance for diagnosis [14].

WHO CNS5 considers all *IDH* mutant diffuse astrocytic tumors as “Astrocytoma, *IDH*-mutant” and are then graded as CNS WHO grade 2, 3, or 4. Furthermore, grading is no longer entirely histological, since the presence of *CDKN2A/B* homozygous deletion results in a CNS WHO grade of 4, even in the absence of microvascular proliferation or necrosis [14].

For a diagnosis of “Glioblastoma, *IDH*-wildtype” the novel WHO CNS5 incorporates 3 genetic parameters (*TERT* promoter mutation, *EGFR* gene amplification, combined gain of entire chromosome 7 and loss of entire chromosome 10) as criteria. For *IDH*-wildtype diffuse astrocytic tumors in adults, several works have shown that the presence of 1 or more of the 3 genetic parameters is sufficient to assign the highest WHO grade [16,17]. Consequently, “Glioblastoma, *IDH*-wildtype” in adults should be diagnosed in the setting of an *IDH*-wildtype diffuse and astrocytic glioma if there is either microvascular proliferation, or necrosis, or *TERT* promoter mutation, or *EGFR* gene amplification, or +7/−10

chromosome copy number changes. In IDH-wildtype diffuse astrocytomas occurring in younger age groups, however, consideration should be given to the different types of diffuse pediatric-type gliomas [14].

3. Neuroimaging

Neuroimaging has transformed neuro-oncology and the way glioblastoma is diagnosed and treated. First, with the advent of Computed Tomography (CT), and subsequently the Magnetic Resonance Imaging (MRI), these technologies have permitted an earlier identification of asymptomatic lesions. Nowadays, imaging is critical for pre-surgical diagnosis, intraoperative management, surgery, and ultimately monitoring after treatment with radiation and chemotherapy [18]. Anatomic imaging remains critical to identifying glioblastomas, but increasingly, advanced imaging methods allowing physiologic imaging have impacted the way these patients are managed [18].

3.1. Computed Tomography

Contrast agent-enhanced CT represented a major advance in modern neuroimaging, permitting an accurate anatomic localization of brain tumors and, by virtue of contrast enhancement, the malignant ones [19]. CT has wider availability, faster scanning times, and lower cost compared with MRI [20]. Despite these benefits, CT requires radiation exposure to the patient, which may be additive if serial imaging is needed. Furthermore, soft tissue resolution on CT is inferior to MR imaging [21]. The development of MRI diffusion-weighted sequences that allowed an indirect estimation of tumor cellularity transformed neuroimaging and replaced CT for the diagnosis of glioblastoma [19].

Still, CT can provide additional information regarding calcification or hemorrhage and be useful for subjects who cannot undergo MR imaging, such as in those with medical implants [18].

3.2. Magnetic Resonance Imaging

MRI is the most widely used, non-invasive technique in the primary diagnosis of brain tumors [2,3]. Although MRI provides very powerful anatomical information, it has proven to be of limited value for diagnosing gliomas in some situations. Specifically, MRI mainly provides detailed morphological information but does not effectively discriminate tumor tissue from concurrent processes such as inflammation, scarring, edema, or bleeding that can lead to incorrect estimates of the actual extension of the tumor mass (Figure 1) [3].

Furthermore, some lesions can be confounded with glioblastoma, including brain abscess (Figure 1), lumps, or space-occupying lesions (Figure 2a,b); certain demyelinating pathologies; the hemorrhagic transformation of stroke (Figure 2); or other lower-grade gliomas or brain tumors including metastases (Figure 3b).

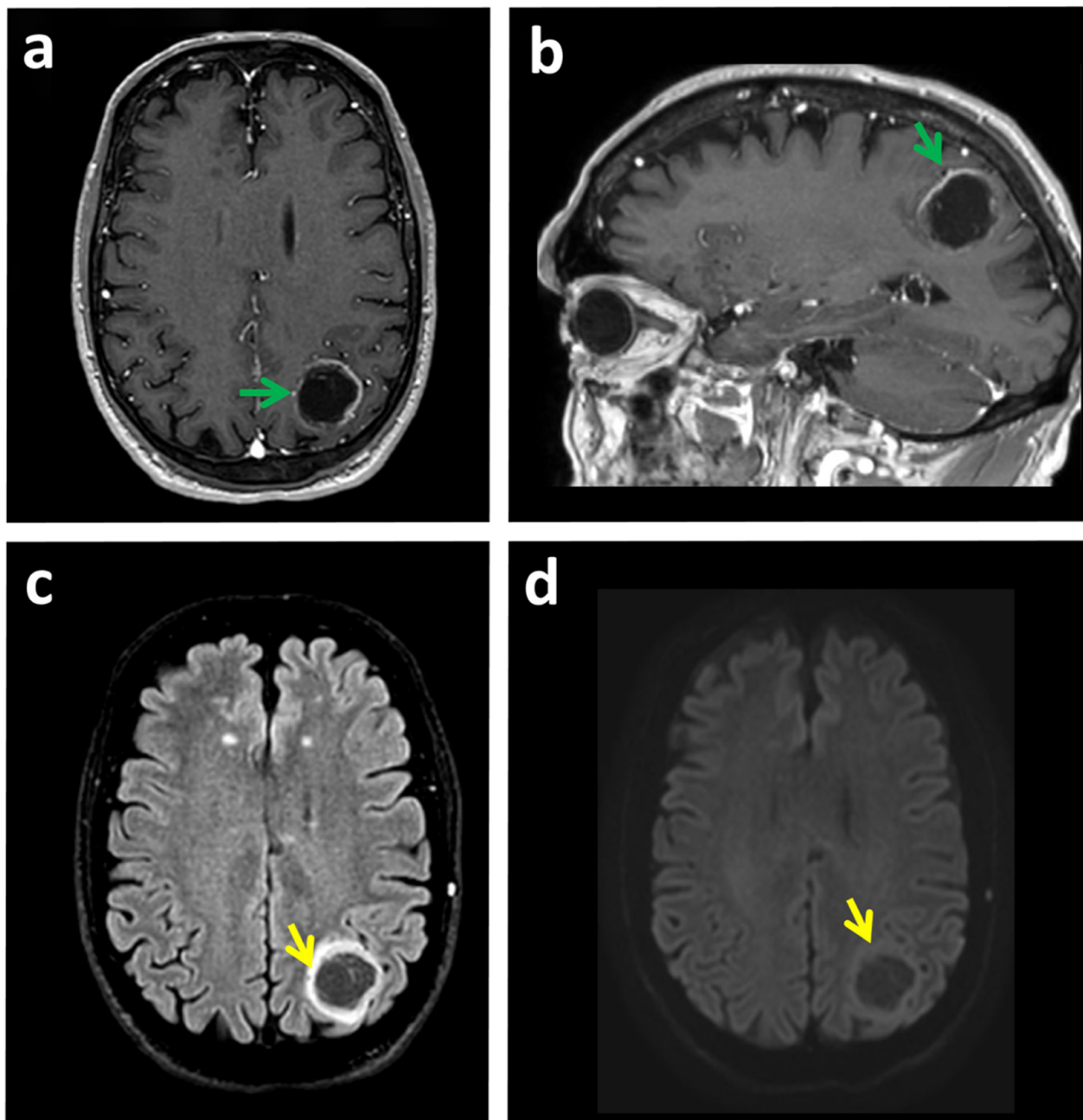


Figure 1. A case of glioma that could be confounded with brain abscess by MRI. (a,b) MRI images of a patient with glioblastoma in the left parieto-occipital lobe. T1W_3D-FFE MRI with gadolinium paramagnetic contrast. (a) Axial and (b) Sagittal reconstruction. The tumor shows contrast rim-enhancement (green arrow). This lesion was confounded with a brain abscess. (c) Fluid-attenuated inversion recovery (FLAIR) shows a parieto-occipital space-occupying lesion with peripheral hyperintensity and central hypointensity (yellow arrow). (d) The diffusion sequence shows minimal restriction of hydric diffusion (yellow arrow), which excludes the possibility that it is an abscess with typical behavior. Biopsy confirmed a diagnosis of glioblastoma.

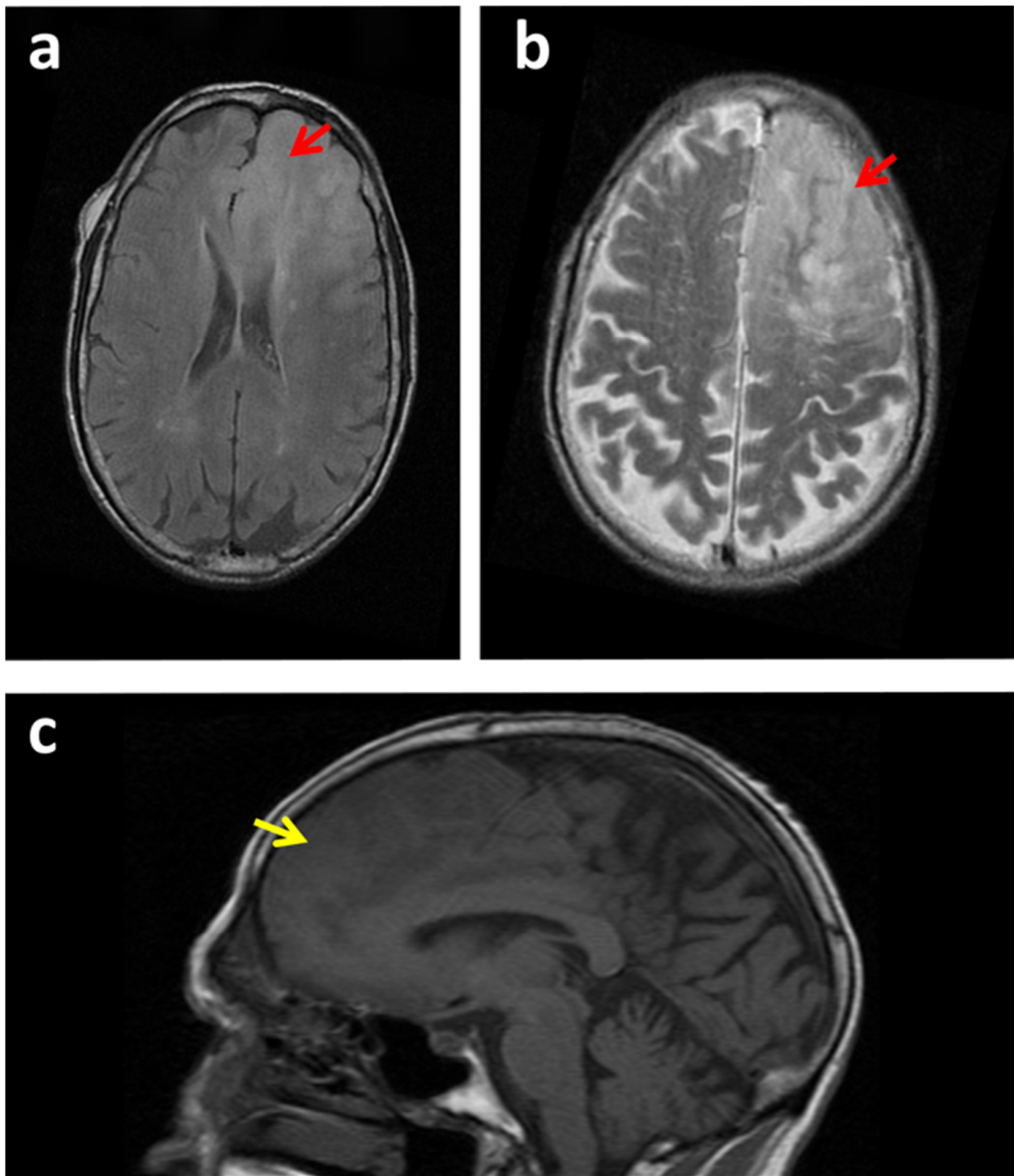


Figure 2. MRI scans of a case of glioma that could be confounded with an ischemic stroke. (a–c) MRI images of a patient with a glioma in the right frontal lobe (red arrows). (a) Inversion recovery fast spin-echo (IRFSE) Fluid-Attenuated Inversion Recovery (FLAIR), axial MRI. (b) Axial FSE T2 MRI image. (c) Spin-echo (SE) T1 sagittal MRI image. The space-occupying lesion could be confounded with an ischemic stroke in evolution (yellow arrows). Loss of gray and white matter differentiation. The lesion was confirmed to be a diffuse tumoral mass compatible with grade II astrocytoma by anatomopathological analysis.

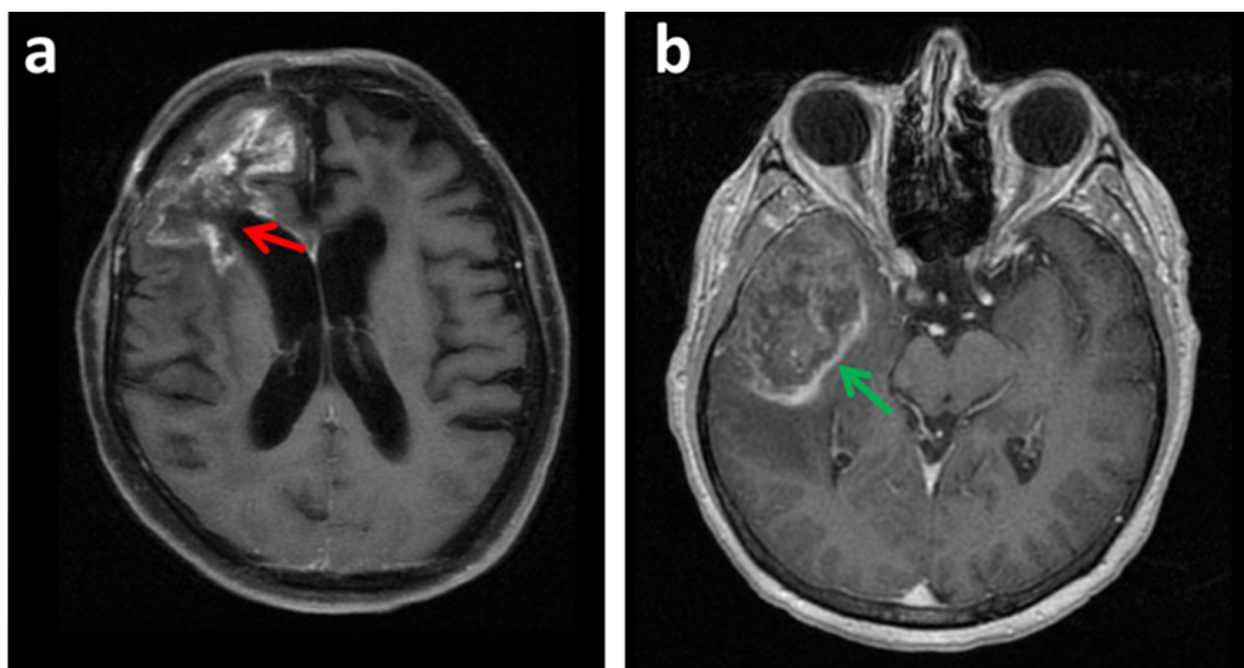


Figure 3. Other lesions can be confounding with glioblastoma. (a) Axial FS T1 MRI image with contrast of a glioblastoma recurrence (red arrow). In some situations, conventional MRI cannot correctly differentiate tumor tissue from post-therapeutic effects following neurosurgical resection and radiation. In this image, tumor recurrence was confounded with treatment necrosis produced by radiation. (b) Axial 3D Fast spoiled gradient echo (FSPGR) with MRI image. A patient suffering from hepatocellular carcinoma (HCC) presented one brain lesion detected by MRI (green arrow). In this situation a glioblastoma could be confounding with a brain metastasis. A biopsy indicated a glioblastoma and was discarded to be a brain metastasis from the HCC.

The ability of conventional MRI to differentiate tumor tissue from post-therapeutic effects following neurosurgical resection, radiation (Figure 3a), alkylating chemotherapy, radiosurgery, and/or immunotherapy is also limited. For instance, the discrimination between tumor recurrence and post-surgical scar tissue is difficult to evaluate by MRI [3].

Although conventional MRI techniques are precious for evaluating the structure and anatomy of the brain, this may not be sufficient for the diagnosis of glioblastoma. Importantly, current improvements in MRI approaches can provide helpful physiological and functional information [22]. The emergence of novel MRI perfusion techniques offers enhanced procedures for tumor grading, guiding stereotactic biopsies, and monitoring treatment efficacy [23]. Perfusion imaging can help in treatment-related decision making, identify treatment-related processes (i.e., radiation necrosis, pseudoprogression, and pseudoregression), and be helpful to differentiate between tumor types and between tumor and non-neoplastic conditions [23].

Due to the limitations of MRI, the final diagnosis of glioblastoma requires a stereotactic brain biopsy and/or post-surgery histopathological analysis. However, glioblastomas present a high intra-tumoral heterogeneity, which undermines the use of a single biopsy for determining the tumor genotype, and has implications for potential targeted therapies [24]. Furthermore, biopsies might promote the natural history of glioblastomas [25,26]. These disadvantages highlight the importance of looking for other molecular-imaging-based technologies that allow efficient and safe diagnosis of these brain tumors.

3.3. Positron Emission Tomography (PET)

PET is routinely used in diagnosing, grading, and staging cancers and in assessing the efficacy of therapies. While MRI provides useful anatomical data, PET provides comple-

mentary biochemical information obtained in a non-invasive manner [27]. PET provides the highest sensitivity and resolution compared to other imaging modalities, allowing for the detection of very small tumors. The development of PET has had broad consequences in clinical practice and has been associated with an estimated change in intended management in about one-third of cases [28].

To date, many PET agents have been developed. The already-established PET tracers are focused on general cancer hallmarks [29] that are not specific to any tumor type. Most of them are sustained proliferation markers that indicate an increase in glucose metabolism, protein synthesis, or DNA replication. Thus, the PET tracers generally consist of radionuclide-labeled forms of the “building blocks” of macromolecules: sugars, amino acids, and nucleotide bases [27]. The gold standard tracer for most PET cancer imaging is 2-[¹⁸F]fluoro-2-deoxy-D-glucose ([¹⁸F]FDG), a fluorine-18 glucose analog [30], being the most widely used in clinical radiopharmaceutical practice, and accounting for more than 90% of total PET scans [31]. There are several tracers based on neutral amino acid analogues, such as [¹¹C]methionine ([¹¹C]MET), [¹⁸F]fluoroethyl-tyrosine ([¹⁸F]FET), [¹⁸F]L-fluoro-dihydroxyphenylalanine ([¹⁸F]FDOPA), or [¹⁸F]fluoro-thymidine ([¹⁸F]FLT), that show high diagnostic performance [27,32]. Another non-aminoacidic tracer that can be used in brain tumors is choline, either as [¹¹C]choline or [¹⁸F]choline, as tumor cells increase choline uptake since they experience high phospholipid turnover in their membranes [32–34]. [¹¹C]choline can be used for tumor monitoring, as it presents high diagnostic accuracy for the differentiation of glioma relapses from radiation-induced necrosis [35], and [¹⁸F]choline could be potentially used as a surgical imaging biomarker, as it was proven helpful for the discrimination of the highly proliferative peripheral area of the tumor and intraparenchymal hemorrhage [36].

The use of metabolic alteration tracers is helpful due to their simplicity, but metabolic changes are not unique to cancers. Hence, although useful in diagnosis, they are most appropriate for disease monitoring. For example, [¹⁸F]FDG is ineffective for diagnosing gliomas due to the high glucose metabolism in the normal brain, which results in suboptimal tumor detection and delineation, especially upon treatment [3,37]. Besides, many PET tracers present a limited blood-brain barrier (BBB) penetration that limits their use for glioblastoma imaging [27]. Other radiotracers for brain tumors are currently under evaluation, and include the glutamine analog 4-¹⁸F-(2S,4R)-fluoroglutamine, which shows high uptake in gliomas but low background brain uptake and may facilitate clear tumor delineation [38].

There are other tracers currently in use that focus on different processes than metabolism [27, 39]. Multiple radiotracers sense oxygen levels, such as [¹⁸F]Fluoromisoindazole ([¹⁸F]FMISO), which can be used to visualize hypoxia [40]. The success of [¹⁸F]FMISO in glioma imaging is limited for its low sensitivity differentiating normoxic and hypoxic tissue and its low BBB permeability [41,42]. Nevertheless, hypoxia imaging can be useful in solid tumors treatment since this biochemical process is critical for monitoring the effective regression after targeted radiotherapy [43].

Another process that is useful for imaging is inflammation, characteristic of glioblastoma pathology. Small molecule inhibitors of the mitochondrial membrane’s translocator protein (TSPO) are also used as PET tracers [44]. Their use in glioblastoma is limited due to the heterogeneity of the tumor and because the signal from tumor-related inflammation cannot be well distinguished from the signal caused by radiation therapy [27].

New PET imaging molecules are being developed hand in hand with new therapeutical advances that target proliferation, immunity, and genetic modifications. These new imaging agents use tumor-specific biomarkers rather than general ligands of proliferation, hypoxia, or inflammation. Some examples, yet to be used in human brain imaging, target sigma 1 (associated with invasiveness), sigma 2 (associated with proliferation), PD-L1 (immune checkpoint), epidermal growth factor receptor (EGFR), ADP-ribose polymerase (PARP), or isocitrate dehydrogenase (IDH), among others [27,45].

There remains an unmet need for highly specific imaging tools that allow for identifying brain tumors at early stages, monitoring changes upon treatment, and determining signs of progression or recurrence. An innovative and attractive alternative is termed “immunotargeted imaging” [46,47]. This approach merges the target selectivity and specificity of antibodies and engineered fragments toward a given tumor cell surface marker with PET imaging techniques to generate “immuno-PET”. By merging the high target specificity of antibodies with the high spatial resolution, sensitivity, and quantitative capabilities of PET, it is possible to conduct the non-invasive diagnosis and monitoring of patients over time using in vivo, integrated, quantifiable, 3D, full-body immunohistochemistry (IHC) as a “virtual biopsy”.

4. Elements of Immuno-PET: Target, Antibody and Radionuclide

We live within a “cancer-omics” revolution that reveals many clinically relevant alterations that are not yet included into the medical practice, at least partly due to the limited number of non-invasive imaging biomarkers [48]. An innovative option, termed “immunotargeted imaging”, merges the target specificity and selectivity of antibodies and derivatives towards a given tumor cell surface marker with the capabilities of a given imaging technique. Immunotargeted imaging by PET necessitates three components that are required to fulfill several characteristics: a suitable target for imaging, an optimally engineered antibody for imaging applications, and selecting an appropriate radionuclide for immuno-PET (Figure 4).

4.1. Selection of an Appropriate Target for Immuno-PET

A suitable epitope for immuno-PET needs: (I) to be exposed on the outer surface of the plasma membrane or to have extracellular components to facilitate the access of the antibody or a derivative, (II) to be highly expressed in the tumor, but (III) to be absent or to present low expression levels in healthy tissue. The target is not limited to malignant cells, it can also be related to different tumor components, including vasculature, stromal cells, and extracellular matrix and infiltrating immune cells [49].

Ideally, a biomarker should provide additional information about the tumor and predict prognosis, survival, or therapeutic outcome. In recent years, several pan-cancer studies have been performed [50]. The growing number of massive glioblastoma-specific databases containing multi-omics data (transcriptome, genome, epigenome, proteome, degradome, kinome, microbiome, metagenome, and metabolome, among others) linked to clinical data [51], together with the development of bioinformatics, facilitates the identification of novel biomarkers that could serve as bases to develop immuno-PET probes to target gliomas.

4.2. Selection of Optimally Engineered Antibody Derivates for Immuno-PET

Antibodies can recognize epitopes with high affinity and specificity. Conventional antibodies present an extended serum half-life that ranges from days up to 3 weeks. This long exposure is a suitable property for antibodies to be used as therapeutics. However, while the exposure of the antibody to the target would be incremented [46,49,52], this could represent a limitation for imaging, as they require several days for being cleared from blood and background for proper visualization by immuno-PET [53].

Ideal immuno-PET imaging requires a highly specific tumor uptake and low background retention of the radiotracer. To this end, a tracer should specifically bind and saturate its target as quickly as possible, and the unbound tracer should be cleared out rapidly from the blood. Protein engineering of antibodies allows the production of smaller fragments maintaining their antigen specificity and affinity with different pharmacokinetics. The clearance of these antibody derivatives can be influenced by their size, surface charge, and hydrophilicity/hydrophobicity, as well as any fused or conjugated molecules [46,49].

Removal of the Fc region results in a faster blood clearance and increased tumor-penetration rate, allowing imaging within several hours after injection [54]. The Fc frag-

ment absence avoids its related specific functions including complement- and effector cell-mediated immune reactions. Moreover, the reduction of the size of antibodies favors its clearance through the renal system (whose protein clearance threshold is ~60 kDa).

In $F(ab')_2$ ($F(ab')_2$ -Fab dimer) and Fab (Fragment antigen-binding) antibody fragments, the CH_2 domain is removed, increasing their blood clearance, allowing a faster visualization and optimizing images. Although $F(ab')_2$ size (~120 kDa) is over the kidney size clearance threshold, both $F(ab')_2$ and Fab fragments are cleared through this pathway. This could be due to the enzymatic cleavage of $F(ab')_2$ into smaller molecules such as Fab, which can pass the glomerular membrane [55,56].

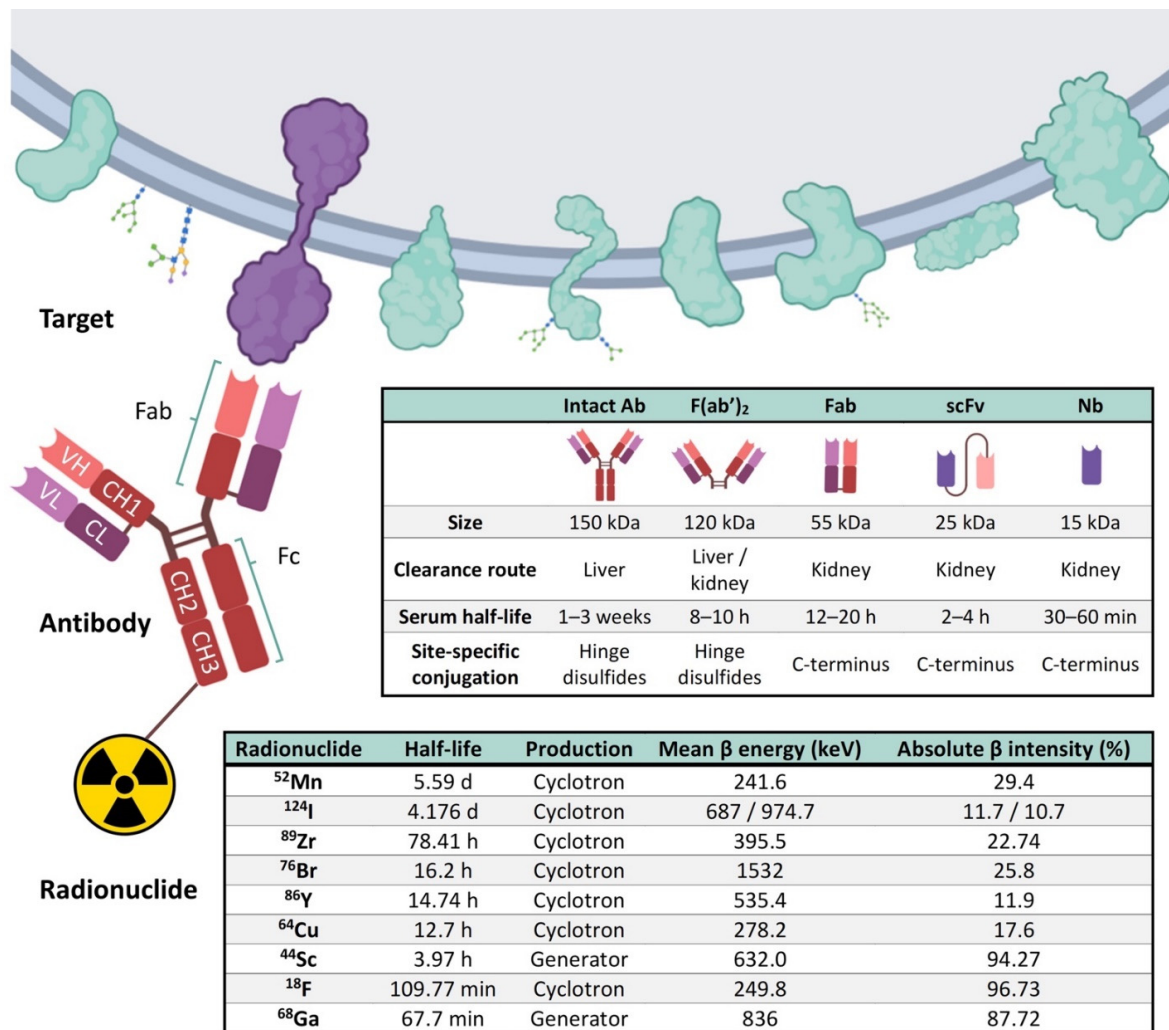


Figure 4. Representation of the three main components of the immuno-PET. Targets present in the external surface of the plasma membrane, antibody, and its derived immune fragments $F(ab')_2$, Fab, scFv, and Nb, and the most commonly used radionuclides are represented. A typical antibody (Immunoglobulin G, IgG) is composed of two heavy (H) chains and 2 light (L) chains. Heavy chains contain a series of immunoglobulin domains, usually with one variable domain (VH) that is important for antigen binding, and several constant domains (CH1, CH2, CH3). Light chains are composed of one variable (VL) and one constant (CL) domain. Abbreviations: Variable (V) and constant (C), Light (L), and Heavy (H); Ab, Antibody; Fab, Fragment antigen-binding; $F(ab')_2$, Fab dimer; scFv, single-chain variable fragment; Nb, Nanobody; ^{18}F , Fluorine; ^{44}Sc , Scandium; ^{52}Mn , Manganese; ^{64}Cu -Copper; ^{68}Ga , Gallium; ^{76}Br , Bromine; ^{86}Y , Yttrium; ^{89}Zr , Zirconium; ^{124}I , Iodine [46,57,58]. Figure adapted with permission from González-Gómez et al. [59]. Image created with BioRender.com (accessed on 6 September 2021).

One of the most common formats is the single-chain variable fragment (scFv, ~25 kDa), which covalently binds a light chain variable domain (VL) with a heavy chain variable domain (VH) through a flexible peptide [60]. Importantly, this linker can be modified to allow cell permeability and BBB penetration [61].

scFvs can also be modified by adding different portions of the constant region (CH), generating different fragments. Diabodies consist of an scFv dimer (Db; ~50 kDa) connected by a short linker that does not permit to pair the two dimers in the same chain; they interact with the antigens in a divalent manner. Minibodies (Mb; ~80 kDa) are fusion proteins composed of an scFv fused to a single Fc [47,53]. The specificity for the antigen remains intact for all these fragments; they also have a better blood clearance and a better background-signal ratio. Moreover, in contrast to complete antibodies, these fragments could pass through the BBB more efficiently [52,62].

Nanobodies (Nb; ~15 kDa) are the single variable domain-heavy chain fragment (VHH) of the heavy-chain-only antibodies (HCAbs) derived from the *Camelidae* species [63]. Variable new antigen receptors (VNARs) derive from the single variable domain of the heavy-chain-only antibodies or immunoglobulin new antigen receptors (IgNARs) of cartilaginous fish [64]. Smaller size and increased plasticity allow nanobodies and VNARs to recognize unique conformational epitopes, including unstructured regions of intrinsically disordered proteins [65] and active sites of enzymes and cavities of receptors [66,67].

Affibodies (AB; ~7 kDa) are nonimmunogenic three-helix scaffold-based derived peptides (~58 amino acids) engineered from the protein A of *Staphylococcus aureus*, which can recognize a wide variety of targets with high affinity [68,69]. Owing to their small size they can access antigens that would be unattainable to conventional Fv-based antibodies and derivatives. However, it is crucial to consider that due to their small size the clearance will be faster than other bigger fragments [68,70]. To prevent unwanted immune responses induced by non-human antibodies and antibody fragment derivatives, these can be “humanized” by modifying their protein sequences [71–73].

4.3. Selection of an Adequate Radionuclide That Fits with the Engineered Antibody Derivates

The third component of the immuno-PET consists of the positron-emitting radionuclide. It is critical to match the biological half-life of the antibody or fragment being used with the physical half-life of the positron-emitting radionuclide. It is also essential that the obtained radioimmunoconjugates preserve their affinity to the target and preserve or improve their properties.

To successfully detect the antibody binding to the target by PET, it is necessary to have a positron-emitter linked to the antibody that has to be in a stable and inert way. For those immune molecules with a long circulating half-life (slow kinetics) such as intact conventional antibodies ($t_{1/2}$ = days to weeks), radionuclides with longer half-lives such as ^{89}Zr ($t_{1/2}$ = 78.4 h) and ^{124}I ($t_{1/2}$ = 100.3 h) will be more suitable [74]. Smaller antibody-derived fragments can be labeled with intermediate half-life radionuclides such as ^{64}Cu ($t_{1/2}$ = 12.7 h) and ^{86}Y ($t_{1/2}$ = 14.7 h), or short half-life such as ^{18}F ($t_{1/2}$ = 110 min), ^{44}Sc ($t_{1/2}$ = 3.94 h), and ^{68}Ga ($t_{1/2}$ = 67.7 min). Due to its small size, affibodies could be combined with isotopes of shorter half-lives, such as ^{18}F and $^{99\text{m}}\text{Tc}$ [68].

Although ^{68}Ga or ^{44}Sc can be produced in a cyclotron [75–78], they can advantageously be produced in a cyclotron-independent manner [79–81]. These radionuclides can be produced in a commercially available $^{68}\text{Ge}/^{68}\text{Ga}$ or $^{44}\text{Ti}/^{44}\text{Sc}$ generator, a result more affordable and accessible to any PET center [79–81].

^{44}Sc presents further advantages allowing multiplexed PET (mPET) imaging. ^{44}Sc emits prompt gamma-rays right after the positron emission that can be distinguished from standard positron emitters such as ^{18}F or ^{68}Ga [80–82], enabling the simultaneous non-invasive imaging of two different radiotracers with PET scanners [81].

Radionuclides can be directly conjugated to the antibody or engineered form (such as ^{18}F , ^{124}I and ^{76}Br by radiohalogenation [83]) or indirectly using a chelating moiety that serves as linkers. The linker contains a chelating group for the attachment of radiometals

and a group that reacts with ϵ -amino groups of lysine residues and/or N-terminus of the antibody form. The most widely used for immuno-PET are siderophore desferrioxamine-B (DFO), hexadentate tris(hydroxamate), 1,4,7,10-tetraazacyclododecane-1,4,7,10-tetraacetic acid (DOTA), and 1,4,7-triazacyclononane-1,4,7-triacetic acid (NOTA), among others [84–86].

Direct and linker-mediated binding of the positron-emitter radionuclide to the antibody can incorporate the tracer at random sites in the protein altering of their antigen-binding site [46]. Further strategies have been designed to conjugate the linker in a site-directed manner to avoid this issue [46,84–86]. These alternatives include click chemistry by biorthogonal reactions between two coupling partners (i.e., alkyne and azide) [87].

Immuno-PET imaging requires simple, fast, and specific radiolabeling of antibody-based probes under mild conditions. Biorthogonal reactions fulfill these criteria, as they can display high selectivity and produce a chemically and biologically inert product/linkage. These selective reactions are kinetically fast and biocompatible, occurring at physiological pH, temperature, and in a physiologically relevant solvent milieu. These quick and modular reactions give high product yields and remain physically stable [88]. Notably, several selective bioorthogonal reactions can occur in living systems, allowing for a two-step pretargeting strategy [89]. In this setting, a primed antibody or subunit, previously linked to one of the reaction components, can be administered prior to completion of the reaction [87,90,91]. Then, the second component (i.e., a linker/chelating agent marked with the radionuclide) can be administered hours to days later depending on the antibody format and clearance route. This strategy permits the use of smaller doses of radioactive material, provides a faster clearance and reduces patients' exposure to radioactivity while providing a better signal-to-noise ratio.

Furthermore, the two-step pretargeting strategy allows the labeling of different tracers (e.g., fluorescent dyes for fluorescence-guided surgery, MRI-tracers such as (Gd)-complexes, or SPIO nanoparticles, among others) to the same pretargeted antibody to generate multimodal and/or multifunctional imaging agents [92,93].

5. Current Perspectives of Immuno-PET for Glioblastoma

Several targets are functionally relevant in glioblastoma, since they have clinical potential as prognostic markers. In addition, they could be used as molecular targets for the delivery of agents for their detection. To date, immuno-PET imaging probes have been mainly designed to target glioblastoma tumors in preclinical models. Several of them have already been successful in detecting gliomas in preclinical studies, as shown in Table 1. These tracers allow for evaluating multiple hallmarks [29] of gliomas and the treatment response in preclinical settings.

Table 1. Immune-PET tracers for glioblastoma.

| PET Imaging Probes | Conjugation Strategy | Targets | Application | Models | References |
|--|-----------------------|---------|---|---|------------|
| [¹⁸ F]AIF-NOTA/NODAGA-PODS-Z-EGFR:03115 (EGFR-targeting affibody molecule) | Cysteine-based random | EGFR | Many EGFR gene alterations have been identified in gliomas, especially glioblastomas. | Subcutaneous xenograft mouse model with U-87 MG vIII cells | [94] |
| [¹²⁴ I]I-PEG ₄ -tptddYddtpt-ch806 (tptddYddtpt is a peptide “clicked” onto dibenzylclooctyne(DBCO)-derivatized ch806) | Click chemistry | EGFR | ch806, an anti-EGFR mAb, can distinguish tumor cells with an amplified/overexpressed EGFR phenotype from normal cells having wild-type levels of EGFR expression. | Subcutaneous xenograft mouse model with U-87 MG.de2-7 cells | [95] |

Table 1. Cont.

| PET Imaging Probes | Conjugation Strategy | Targets | Application | Models | References |
|---|----------------------|----------------|---|--|------------|
| [⁴⁴ Sc]Sc-CHX-A''-DTPA-Cetuximab-Fab | Lysine-based random | EGFR | Radiolabeling and preclinical evaluation of ⁴⁴ Sc-labeled protein molecules. | Subcutaneous xenograft mouse model with U-87 MG | [96] |
| [⁸⁹ Zr]Zr-DFO-cetuximab | Lysine-based random | EGFR | ⁸⁹ Zr-cetuximab was used to assess transient BBB disruption in vivo permeability induced by the combination of injected microbubbles with low intensity focused ultrasound. | Orthotopic murine glioma with GL261 cells | [97] |
| [⁶⁴ Cu]Cu-NOTA-Bs-F(ab) ₂ (bispecific immunoconjugate by linking two antibody Fab fragments, an anti-EGFR and an anti-CD105) | Lysine-based random | EGFR and CD105 | EGFR has been extensively studied as a target for anticancer therapy, and its activation stimulates tumor proliferation and angiogenesis. Similarly, CD105 (also called endoglin) is abundantly expressed on activated endothelial cells, and such over-expression is an adverse prognostic factor in many malignant tumor types. | Subcutaneous xenograft mouse model with U-87 MG | [98] |
| [⁶⁴ Cu]Cu-NOTA-EphA2-4B3 (human anti-EphA2 mAb) | Lysine-based random | EphA2 | EphA2 receptor tyrosine kinase is overexpressed in several tumors, including glioblastoma. | Orthotopic brain glioblastoma murine models (two patient-derived cell lines and U-87 MG cells) | [99] |
| [⁸⁹ Zr]Zr-DFO-mCD47 | Lysine-based random | CD47 | CD47 is a membrane protein overexpressed on the surface of most cancer cells. It is involved in the increase in intracellular [Ca ²⁺] that occurs upon cell adhesion to the extracellular matrix and is also a receptor for the C-terminal cell-binding domain of thrombospondin. | Orthotopic murine glioma with GL261 cells | [100] |

Table 1. Cont.

| PET Imaging Probes | Conjugation Strategy | Targets | Application | Models | References |
|--|----------------------|---------|---|--|------------|
| [⁶⁴ Cu]Cu-NOTA-AC133 (anti-AC133 mAb) | Lysine-based random | AC133 | AC133 is an N-glycosylation-dependent epitope of the second extracellular loop of CD133/prominin-1, a cholesterol-binding protein of unknown function that locates to plasma membrane protrusions. AC133 ⁺ tumor stem cells have been described for glioblastoma multiforme. | Orthotopic and subcutaneous xenograft mouse models with NCH421k and U-251 MG cells | [101] |
| [⁸⁹ Zr]Zr-DFO-bevacizumab (humanized anti-VEGF) | Lysine-based random | VEGF | ⁸⁹ Zr-labeled bevacizumab was used to assess BBB opening with mannitol. | C3HeB/FeJ mice without tumors | [102] |
| [⁶⁸ Ga]Ga-DOTA-bevacizumab (humanized anti-VEGF) | Lysine-based random | VEGF | ⁶⁸ Ga-labeled bevacizumab was used to assess BBB opening with focused ultrasound exposure in the presence of microbubbles. | Orthotopic murine glioma with U-87 MG cells | [103] |
| [⁸⁹ Zr]Zr-DFO-YY146 (anti-CD146 mAb) | Lysine-based random | CD146 | CD146 plays an important role in several processes involved in tumor angiogenesis, progression, and metastasis. Its expression has been correlated with aggressiveness in high-grade gliomas. | Subcutaneous xenograft mouse model with U-87 MG and U251 cells | [104] |
| [⁶⁴ Cu]Cu-NOTA-YY146 (anti-CD146 mAb) | Lysine-based random | CD146 | CD146 plays an important role in several processes involved in tumor angiogenesis, progression, and metastasis. Its expression has been correlated with aggressiveness in high-grade gliomas. | Orthotopic and subcutaneous xenograft mouse models with U-87 MG and U-251 MG cells | [105] |
| [⁶⁴ Cu]Cu-NOTA-61B (human anti-Dll4 mAb) | Lysine-based random | Dll4 | Dll4 plays a key role to promote the tumor growth of numerous cancer types. | Subcutaneous xenograft mouse model with U-87 MG | [106] |

Table 1. Cont.

| PET Imaging Probes | Conjugation Strategy | Targets | Application | Models | References |
|--|----------------------|-------------------|---|--|------------|
| ^{89}Zr]Zr-DFO-LEM2/15 (anti-MM1-MMP mAb) | Lysine-based random | MT1-MMP/ MMP14 | MMP14 is a metalloprotease frequently overexpressed in many tumors, and it is associated with tumor growth, invasion, metastasis, and poor prognosis. | Xenograft mice bearing human U251 cells and two orthotopic brain glioblastoma murine models (patient-derived TS-543 neurospheres and U-251 MG cells) | [107] |
| ^{89}Zr]Zr-DFO-fresolimumab (human IgG4 mAb, 1D11) | Lysine-based random | TGF β | TGF β mediates extracellular matrix (ECM) remodeling, angiogenesis, and immunosuppression, and regulates tumor cell motility and invasion. | Orthotopic murine glioma with GL261 and SB28 cells | [108] |
| ^{89}Zr]Zr-DFO-fresolimumab (human IgG4 mAb, 1D11) | Lysine-based random | TGF β | TGF β mediates ECM remodeling, angiogenesis, and immunosuppression, and regulates tumor cell motility and invasion. | Patients with recurrent high-grade glioma | [109] |
| ^{89}Zr]Zr-DFO-F19 (anti-FAP monoclonal antibody) | Lysine-based random | FAP | FAP, a 170 kDa type II transmembrane serine protease, is expressed on glioma cells and within the glioma tumor microenvironment. | Subcutaneous xenograft mouse model with U-87 MG cells | [110] |
| ^{89}Zr]Zr-DFO-PD-1 | Lysine-based random | PD-1 | ^{89}Zr labeled α PD-1 antibody was used to assess focal BBB permeability induced by high-intensity, focused ultrasound. | Orthotopic murine glioma with G48a cells | [111] |
| ^{68}Ga]Ga-NOTA-Nb109 (anti-PD-L1 nanobody) | Lysine-based random | PD-L1 | Evaluate the specific affinity of ^{68}Ga -NOTA-Nb109 to several cancer cell lines that expressed endogenous PD-L1. | Subcutaneous xenograft mouse model with U-87 MG cells | [112] |
| ^{89}Zr]Zr-DFO-169 cDb (anti-CD8 cys-diabody) | Lysine-based random | CD8 | Proof-of-concept to detect CD8+ T cell immune response to oncolytic herpes simplex virus (oHSV) M002 immunotherapy in a syngeneic glioblastoma model. | Orthotopic syngeneic murine glioma with GSC005 cells | [113] |
| ^{89}Zr]Zr-DFO-CD11b | Lysine-based random | CD11b | The most abundant population of immune cells in glioblastoma is the CD11b ⁺ tumor-associated myeloid cells. | Mice bearing established orthotopic syngeneic GL261 gliomas | [114] |

Table 1. Cont.

| PET Imaging Probes | Conjugation Strategy | Targets | Application | Models | References |
|--|----------------------|---------|---|---|------------|
| $^{89}\text{Zr}/^{177}\text{Lu}$ Zr/Lu-Lumi804-CD11b | Lysine-based random | CD11b | Theranostic approach for monitoring and reducing tumor-associated myeloid cells in gliomas to improve immunotherapy responses. | Mice bearing established orthotopic syngeneic GL261 gliomas | [115] |
| ^{89}Zr Zr-DFO-OX40 | Lysine-based random | CD134 | CD134 (or OX40) is an activated T-cell surface marker, known to be a costimulatory transmembrane molecule of TNF superfamily, primarily expressed on activated effector T cells and regulatory T cells. | Mice bearing established orthotopic GL261 gliomas | [116] |

Abbreviations: CD8—Cluster of differentiation 8; CD11b—Integrin αM ; CD47—Cluster of differentiation 47; CD105—endoglin; CD134—Tumor necrosis factor receptor superfamily, member 4 (TNFRSF4); CD146—Cluster of Differentiation 146; DLL4—Delta-Like Ligand 4; EGFR—Epidermal Growth Factor Receptor; EPHA2—Ephrin type-A receptor 2; FAP—Fibroblast activation protein alpha; MT1-MMP/MMP14—Membrane-type 1 matrix metalloproteinase; PD-1—programmed cell death receptor-1; PD-L1—Programmed cell death ligand 1; TGF β —Transforming growth factor β ; VEGF—Vascular Endothelial Growth Factor.

Several immuno-PET tracers' [94–101,106,107] target membrane proteins whose expression is altered in glioblastoma including the Epidermal Growth Factor Receptor (EGFR), Delta-Like Ligand 4 (DLL4), Ephrin type-A receptor 2 (EPHA2), Cluster of differentiation 47 (CD47), the AC133 antigen, and the Membrane-type 1 matrix metalloproteinase (MT1-MMP/MMP14) (Figure 5). In vivo administration of these tracers showed high-specific-contrast imaging of the target in an MT1-MMP expressing glioblastoma tumor model and provided strong evidence for their utility as an alternative to non-specific imaging of glioblastoma.

Glioblastomas develop in complex tissue environments, which support sustained growth, invasion, progression, and response to therapies [117]. Several components of the tumor microenvironment such as vessels [108–110], macrophages, and extracellular matrix proteins [104,105] are also promising candidates for the development of immuno-PET diagnostic approaches in glioblastoma [108–110,114].

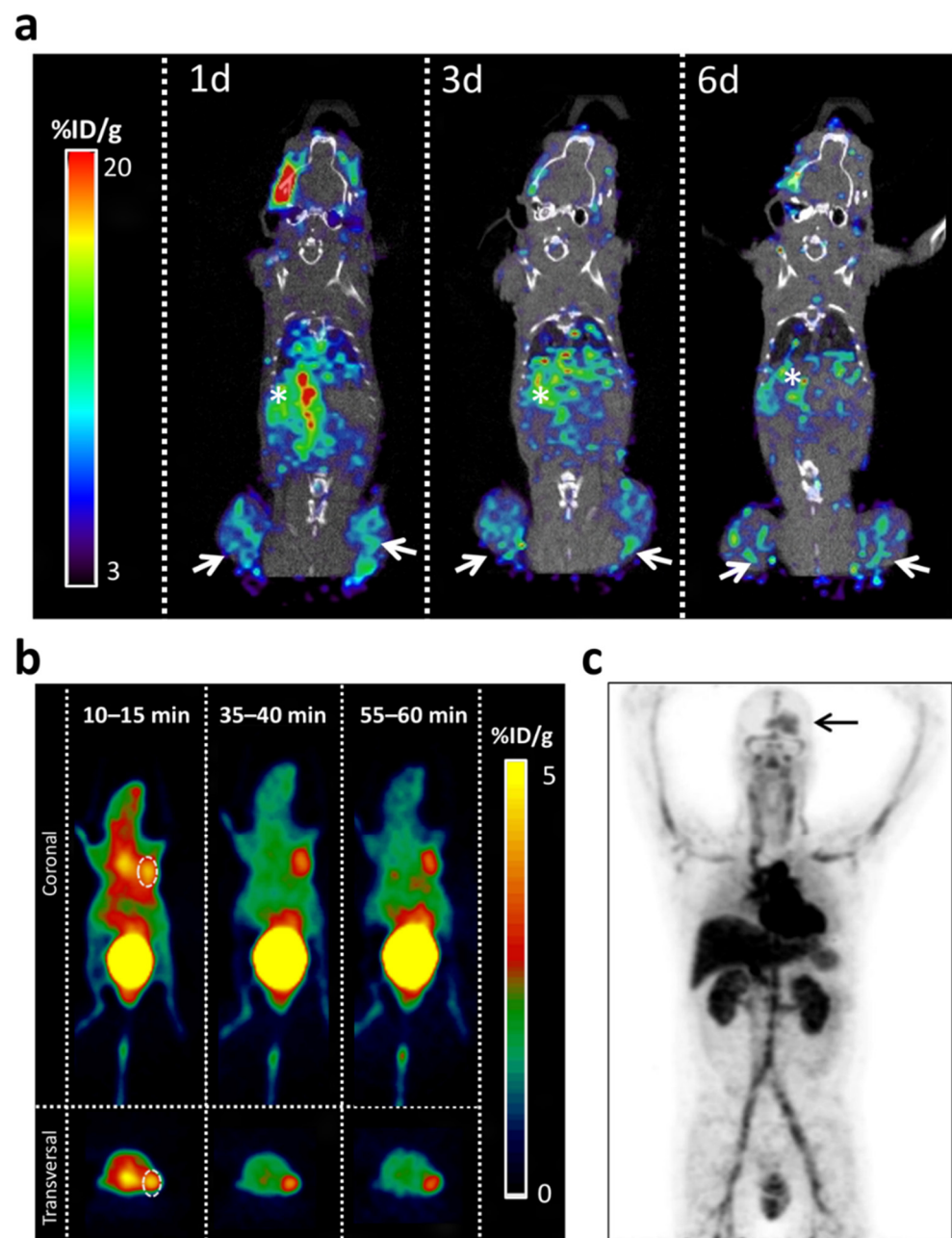


Figure 5. Examples of immuno-PET applications for the diagnosis of glioblastoma in preclinical models and patients. (a) PET/CT imaging with radiolabeled [^{89}Zr]Zr-DFO-LEM 2/15 in a mouse bearing heterotopic xenografts containing patient-derived neurospheres. To generate subcutaneous heterotopic xenografts, 250,000 cells (MT1-MMP+, TS-543) were resuspended in 200 μL of a 1:1 mix of DMEM (Sigma, St. Louis, MO, USA) with Matrigel (BD Biosciences, San Jose, CA, USA). Next, the Matrigel:DMEM-cells mixture was injected subcutaneously into the flanks of 6 weeks athymic nude mice (Nude-Foxn1nu, Harlan Laboratories). Tumors were allowed to develop until palpable prior to immuno-PET analysis. Mice were inoculated with 2,3 MBq of [^{89}Zr]Zr-DFO-LEM2/15 by retro-orbital sinus injection. (a–c) Representative fused PET/CT images. Sagittal whole-body sections at 1 (1d), 3 (3d) and 6 (6d) days post-injection. Images were obtained with a small-animal Argus PET-CT scanner (SEDECAL, Madrid, Spain). The PET studies (energy window 250–700 KeV and 30 min static acquisition) and CT (voltage 45 kV, current 150 μA , 8 shots, 360 projections and standard resolution) were performed at various time points post-injection in mice anesthetized by inhalation of 2–2.5% Isoflurane. The PET images were reconstructed using a 2D-OSEM (Ordered

Subset Expectation Maximization) algorithm (16 subsets and two iterations), with random and scatter correction. Tissue activity is expressed as the percentage injected dose per gram of tissue (%ID/g). White arrows indicate the tumors' location. White asterisk indicates the liver. Note the activity of the liver (asterisk) decreases gradually with time while it is maintained in the tumors (arrows). (b) MicroPET imaging of U87-MG xenograft model with [⁶⁸Ga]Ga-NOTA-Nb109. Representative PET images obtained at different time points after injection. The tumor was denoted with a dotted line circle. Reprinted with permission from search was originally [112] 2021 Springer. The labeling of his panel was adapted for formatting. (c) Representative example of [⁸⁹Zr]-Zr-DFO-fresolimumab PET on day 4 and uptake in brain tumor (arrow) in a human patient. Adapted with permission from ref. [109] 2015 SNMMI.

Re-education of the tumor microenvironment of glioblastomas emerges as a novel opportunity for therapeutic intervention, as it has anti-tumorigenic effects [118,119].

Macrophages and microglia accumulate with glioblastoma progression and can be targeted via inhibition of Colony-Stimulating Factor-1 Receptor (CSF-1R) to regress high-grade tumors in animal models of glioblastoma [118,119]. A recent immuno-PET tracer targeting the Integrin α M (CD11b) expressing cells (macrophages) with high specificity in a mouse model of glioblastoma was developed, demonstrating the potential for non-invasive quantification of tumor-infiltrating CD11b+ immune cells during disease progression and immunotherapy in patients suffering of glioblastoma [99,114]. Another anti-CD11b tracer has been shown to be effective in mouse models for imaging tumor-associated myeloid cells (TAMCs), which constitute up to 40% of the cell mass of gliomas [115].

Immunotherapy, especially immune-checkpoint inhibitors, is transforming oncology. Despite glioblastomas frequently express the programmed cell death ligand 1 (PD-L1), the results obtained with anti-PD1 therapy are below expectations. The frequent intra-tumor variability of PD-L1 expression carries significant implications for determination accuracy. PET imaging of immune-checkpoint inhibitors may serve as a robust biomarker to predict and monitor responses to these immunotherapies, complementing the existing immunohistochemical techniques [120].

Other immuno-PET tracers targeting immune cells have been evaluated. A tracer targeting CD8+ T cell immune response to oncolytic herpes simplex virus (oHSV) M002 immunotherapy was evaluated as a proof of concept in a syngeneic glioblastoma model [113]. Another monoclonal antibody-based tracer was developed for immuno-PET imaging of T-cell activation targeting the costimulatory receptor OX40, and used to monitor the stimulated T-cell response in a murine orthotopic glioma model [116].

Furthermore, some of these immuno-PET tracers are valuable tools to determine the transient BBB disruption and permeability induced by mannitol [102] or produced by the combination of injected microbubbles with low-intensity focused ultrasound in vivo [97,103,111]. Notably, [⁸⁹Zr]Zr-DFO-fresolimumab, an immuno-PET tracer based on a monoclonal antibody that can neutralize all mammalian isoforms of TGF- β , was assayed in humans and penetrated recurrent high-grade gliomas (Figure 5c) but did not result in clinical benefit [109].

6. Novel Nanobody-Based Immuno-PET Imaging Methods for Glioblastoma

The development of immuno-PET probes for the diagnosis of glioblastoma may encounter several hurdles to be reached due to the intracranial location of this tumor type. CNS barriers may limit the delivery of conventional antibody-based immuno-PET probes. The restricted entrance of molecules into the CNS is exerted mainly by the blood–brain barrier (BBB) and the blood–cerebrospinal fluid (CSF) barrier (BCSFB) [121]. These dynamic interfaces allow the exclusive passage from the blood into the CNS of receptor-specific ligands and small molecules (MW < 400 Da) that are lipid-soluble [122,123]. The delivery of peptide and protein drugs through the BBB is a major challenge for treating CNS diseases, and strategies to achieve therapeutic concentrations are under development [124]. In this regard, only 0.01–0.4% of the total amount of administered therapeutic antibodies have access to the CNS through passive diffusion [125,126]. Transport of therapeutic antibodies, mostly with the IgG isotype (150 kDa), may be hampered by the binding of their Fc domain

to Fc receptors in the BBB [127]. Both the Fc γ receptor (Fc γ R) and neonatal Fc receptor (FcRn) have been implicated in the inverse transport of IgG through the BBB and their subsequent return from the brain to blood circulation [128,129]. Nevertheless, recent studies have proposed that antibody transcytosis across the BBB is carried by non-saturable, non-specific, Fc-independent mechanisms [130]. These mechanisms may hinder the diagnostic potential of monoclonal antibody-based immune-PET tracers for glioblastoma patients.

The development of antibody subunits targeting glioblastoma biomarkers that overcome the BBB selectivity emerges as a promising tool that could contribute to glioblastoma diagnosis by immuno-PET [131]. Single-domain antibodies (sdAbs) such as nanobodies have a lower MW, enabling better BBB penetrance, tumor uptake, and faster blood clearance than monoclonal antibodies [132,133]. Nanobodies are the single variable domain of the heavy-chain-only antibodies of *Camelidae* (camel, dromedary, llama, alpaca, vicuñas, and guanacos) [63,134]. Nanobodies constitute the smallest molecules derived from antibodies (diameter of 2.5 nm and height of 4 nm; 15 kDa), although they still conserve full antigen-binding capacity with high specificity and affinity [135]. Nanobodies exert low toxicity and immunogenicity. Nanobodies have demonstrated their potential utility in diagnosing, monitoring, and therapy of a wide range of diseases [136,137]. Several differentially expressed proteins have been identified as glioblastoma targets with potential tumor-class predictive biomarker values [138,139]. Furthermore, a wide range of nanobodies targeting glioblastoma targets that have shown cytotoxic effects might constitute potential candidates for developing nanobody-based molecular imaging probes. Candidate nanobodies for immuno-PET approaches recognize molecular targets which play important roles in protein biosynthesis (TUFM, TRIM28), DNA repair and cell cycle (NAP1L1), and cellular growth and maintenance (EGFR, DPYSL2, β -Actin) [140–142]. Recently, a PD-L1-targeting nanobody-based tracer was evaluated to assess the changes in PD-L1 expression sensitively and specifically in different cancer types, which could help screen patients with high expression and guide PD-L1-targeting immunotherapies (Table 1) [112] (Figure 5b).

In contrast to conventional antibodies, nanobody-based immuno-PET probes may launch a novel era for the diagnosis of glioblastoma. Various molecular mechanisms for the transportation of nanobodies through the BBB have been extensively described [143–146] (Figure 6). Receptor-mediated transcytosis performs the movement of receptor ligands (e.g., transferrin, lactoferrin) across the BBB by a specific affinity-dependent unidirectional transport [147,148]. Nanobody FC5 (GenBank no. AF441486), the first nanobody described to traverse the BBB, binds the alpha(2,3)-sialoglycoprotein receptor in the brain endothelium [149,150]. FC5 set the basis for delivering BBB-impermeable therapeutic agents into the brain parenchyma by exploiting the receptor-mediated transcytosis of nanobodies [151]. Adsorptive-mediated transcytosis triggers the transport of basic molecules by electrostatic interactions with anionic microdomains on the cell membrane [152,153]. Several nanobodies with high isoelectric points (pI~9.5) have reported spontaneous delivery into the brain parenchyma. Basic nanobodies mVHH E9 (pI = 9.4), R3VQ (pI > 8.3), and A2 (pI > 9.5) have been shown to traverse the BBB and specifically label their molecular brain targets in vivo [154,155]. Transcytosis of nanobodies may be improved by other molecular shuttles such as peptide-decorated liposomes and cell-penetrating peptides (CPPs), which interact with the endothelial cells of the BBB and undergo nanobody internalization into the brain parenchyma [156–158].

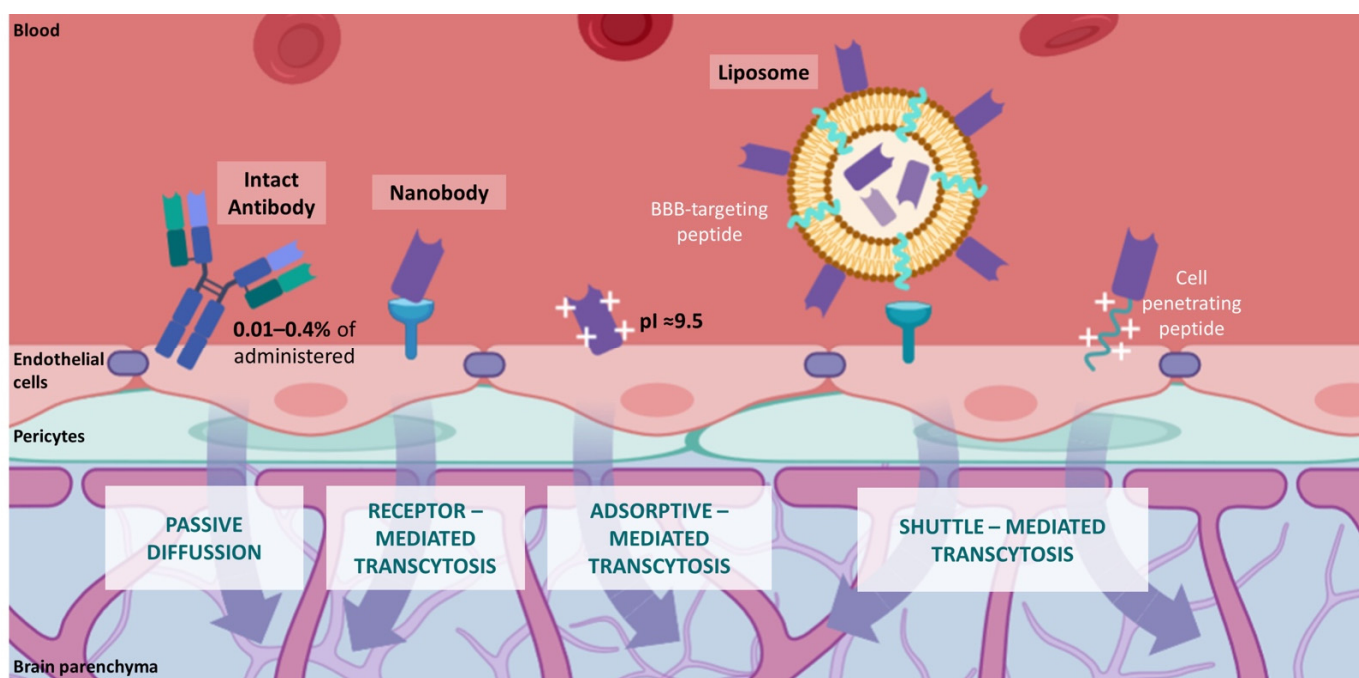


Figure 6. Molecular mechanisms of BBB permeability to antibodies. Comparison of conventional IgG antibodies (passive diffusion) and nanobodies (transcytosis mediated by BBB receptors, adsorptive processes, and BBB shuttle molecules). Image created with [BioRender.com](https://www.biorender.com) (accessed on 6 September 2021).

In this regard, nanobodies crossing the BBB can be utilized as the targeting moieties of diagnostic and/or therapeutic immuno-PET tracers for CNS diseases. Nanobodies have already been used as non-invasive probes in several imaging techniques to visualize molecular pathologies, including glioblastoma [159]. First attempts labeled nanobodies with fluorescent dyes to perform *in vivo* optical imaging. The named EG2 nanobody and its bivalent (EG2-hFc) and pentavalent (V2C-EG2) formats were conjugated to the near-infrared (NIR) Cy5.5 fluorophore and successfully detected EGFRvIII expressing tumors in orthotopic mouse models of glioblastoma by NIR fluorescence imaging [160]. Similar results were obtained with the derivative nanobody EG2-Cys, labeled with NIR quantum dot Qd800 [161]. Cy5.5-labeled VHH 4.43, a nanobody directed against insulin-like growth factor-binding protein 7 (IGFBP7), was able to selectively detect blood vessels of glioblastoma after systemic injection in orthotopic glioblastoma bearing mice [162]. In addition, nanobodies have exhibited applicability as tracers in magnetic resonance imaging (MRI). Small unilamellar vesicles decorated with high Gd payload (Gd-DPTA), Cy5.5, and anti-IGFBP7 were used for dual (optical and MRI) *in vivo* imaging of glioblastoma orthotopic models [163]. Glioblastoma immuno-PET probes based on nanobodies targeting the hepatocyte growth factor (HGF) have demonstrated diagnostic potential in preclinical models. Nanobodies 1E2 and 6E10, linked to an albumin-binding nanobody (Alb8) and labeled with the positron emitter ^{89}Zr , assessed HGF expression in xenografted glioblastoma mouse models [164]. These nanobody-based immuno-PET probes showed therapy potential as they delayed tumor growth. Other nanobody-based probes have evidenced diagnostic properties by performing MRI (R3VQ-S-(DOTA/Gd)₃) [165] and micro-SPECT imaging (^{111}In In-DTPA-pa2H [156]; (^{111}In In-DTPA-pa2H-Fc [166]) of Alzheimer's disease mouse models. These examples highlight the importance of the innovative field of immuno-PET tools based on the diagnostic potential of nanobodies for nuclear imaging and image-guided surgery [167].

Nanobodies have already evinced their clinical benefit in patients. In 2019, the Food and Drug Administration (FDA) and, more recently, the European Medicines Agency

(EMA), approved the use of ALX-0681 (Caplacizumab; Ablynx NV, Ghent, Belgium) for adult patients with acquired thrombotic thrombocytopenic purpura [168,169]. ALX-0681 was the first nanobody reaching the clinic field, paving the way for a new era of diagnostics and therapeutics based on nanobodies. Nanobody-derived immuno-PET tracers are advancing through clinical trials. A human epidermal growth factor receptor 2 (HER2)-targeting nanobody ($[^{68}\text{Ga}]\text{Ga-NOTA-anti-HER2 VHH1}$) has demonstrated its efficient diagnosis of primary breast carcinoma patients by PET/CT in a phase I study [170]. This nanobody-based tracer is being evaluated for the detection of breast-to-brain metastasis in a phase II trial (ClinicalTrials.gov NCT03331601). Recently, a phase I study was conducted to analyze the diagnostic potential of a $^{99\text{m}}\text{Tc}$ labeled anti-PD-L1 nanobody ($[^{99\text{m}}\text{Tc}]\text{Tc-NM-01}$) in non-small cell lung cancer patients by SPECT/CT imaging [171]. Nanobodies constitute a promising toolbox for innovative opportunities in the immuno-PET field towards personalized medicine.

7. Discussion

The current diagnosis of glioblastoma by conventional imaging methods presents multiple limitations. The most widely used technique in the primary diagnosis of this tumor is MRI [2,3]. While it provides very relevant anatomical information, it has a limited value for the diagnosis of glioblastoma because it mainly provides morphological information and does not allow proper discrimination of the tumoral tissue from concurrent processes such as inflammation, scar, edema, or bleeding that can lead to under or overestimate of the actual extension of the tumoral mass. Furthermore, some lesions, including brain abscess, lumps or space-occupying lesions, some pathologies coursing demyelination, the hemorrhagic transformation of stroke, or other lower-grade gliomas can be confounded with glioblastoma. The capacity of conventional MRI to differentiate tumor tissue from post-therapeutic effects following neurosurgical resection, radiation, alkylating chemotherapy, radiosurgery, and/or immunotherapy is also limited. Frequently, the discrimination between tumor recurrence and scar tissue is hard to determine by MRI after surgery [3]. As described above, other routinely neuroimaging techniques (CT, PET) used for the diagnosis of brain tumors also present multiple limitations.

While these imaging techniques are in continuous evolution and will benefit from the development of artificial intelligence [18,172] and bioinformatics, all these disadvantages highlight the importance of looking for other molecular-imaging-based technologies that allow the efficient and safe diagnosis of these brain tumors. Novel targeted imaging tools are needed to identify brain tumors at early stages, evaluate treatment response, and determine signs of progression or recurrence.

Despite continuous advances in the molecular classification [12–14] of gliomas, there have been no major improvements in patient survival over the past decades. There is an urgent need to integrate many clinically relevant alterations and biomarkers found in the multi-“omics” of cancer that are not yet included into the clinical management of glioblastoma patients due, in part, to the limited number of non-invasive biomarkers.

Current quantification of biomarkers in glioblastoma requires immunohistochemistry (IHC) and molecular biology analysis of surgical biopsies. However, this procedure is invasive and is not always feasible for all patients. Notably, the snapshot of a single biopsy usually does not capture the heterogeneity of glioblastomas, and several surgical biopsies and histopathological confirmation are required for a proper diagnosis. Some cases include cytology analysis of the cerebrospinal fluid (CSF); however, these techniques have limited sensitivity [173]. These hurdles represent a clinical challenge and an important risk for the patients leading to a lack of information about their glioblastomas.

Liquid biopsies are non-invasive tools that can provide longitudinal information about the tumor genomic landscape and facilitate the clinical management of patients. They analyze biomarkers present in the body fluids such as blood, urine, saliva, and CSF [174,175]. These biomarkers include circulating tumor cells, exosomes, and circulating tumor DNA (ctDNA) [174,175]. Detecting biomarkers in the blood is beginning a revolution

that is transforming cancer diagnosis for multiple tumor types. However, the blood may not be a suitable source of ctDNA from patients with intracranial tumors, since ctDNA levels are infrequently detected in plasma. While ctDNA is detectable in the plasma of more than 75% of patients with advanced extracranial cancers, it is detectable in less than 10% of glioma patients [176,177].

The CSF is a source of ctDNA that can be sequenced and can reveal tumor heterogeneity providing diagnostic and prognostic information [173]. CSF-ctDNA liquid biopsies face multiple challenges including standardization of protocols, more extensive studies with more patients, and the implementation of well-designed and controlled clinical trials [173]. These hurdles need to be overcome to translate research findings into a tool for clinical practice [173].

Immuno-PET represents an attractive and innovative option for the diagnosis of gliomas allowing the analysis of biomarkers in a non-invasive manner. It combines the target selectivity and specificity of antibodies and subunit toward a biomarker with the high sensitivity, spatial resolution, and quantitative capabilities of PET. The development of novel immuno-PET tools will make it possible to conduct the non-invasive diagnosis and monitoring of patients over time using *in vivo*, quantifiable, 3D, whole body IHC [178], like a “virtual biopsy.” Immuno-PET will complement liquid biopsies to localize and characterize the gliomas and guide subsequent treatment decisions [179].

To date, several immuno-PET imaging tracers have been designed to target glioblastoma and have already proven successful in detecting gliomas in multiple preclinical models. These tracers target membrane proteins whose expression is altered in glioblastoma (including the EGFR, DLL4, EPHA2, CD47, AC133 antigen, and MT1-MMP) [94–101,106,107]: several components of the tumor microenvironment including vessels, macrophages, and extracellular matrix proteins [104,105,108–110,114]. Notably, [⁸⁹Zr]Zr-DFO-fresolimumab, an immuno-PET tracer based on a monoclonal antibody that can neutralize all mammalian isoforms of TGF- β was assayed in humans, penetrated recurrent high-grade gliomas but did not result in clinical benefit [109]. Other immuno-PET tracers can serve to evaluate novel therapies [97,103,111,120] and to evaluate BBB disruption and permeability [108,114,125].

Targeted-radionuclide therapy is a strategy for the treatment of glioblastoma. This nuclear medicine approach enables the visualization of molecular biomarkers and pathways on a subcellular level using a biochemical vector coupled to a radionuclide that could work either for diagnosis (positron- or gamma-emitter) or for therapy (auger electrons-, β^- - or α -emitter) [180]; when the radionuclides are used for the paired imaging and therapy agents, the strategy is called “radiotheranostics”. In the past years, targeted-radionuclide therapy has been used under a palliative context demonstrating to prolong overall survival, progression-free survival, and improve the patients’ life quality [181].

The administration of targeted-radionuclide therapy requires to confirm the presence of the glioblastoma target to determine on treatment options. To this end, immuno-PET emerges an opportunity as a possible quantitative imaging procedure to investigate the different biological properties and pharmacokinetics of tumor-targeted radiolabeled macromolecules including antibody fragments or engineered antibodies.

In addition to antibodies, multiple molecules (chemical, peptides, nanoparticles) have been designed to target specific biomarkers in the gliomas to develop probes of interest that can now be non-invasively imaged with multimodality molecular imaging techniques including MRI, CT, PET, single-photon emission computed tomography (SPECT), bioluminescence imaging, and near-infrared fluorescence to guide targeted therapies with a potential survival benefit and monitor patients’ response [182].

BBB permeability to the antibody-based probes remains a hurdle for immuno-PET applications. Glioblastomas are highly infiltrative and frequently alter the integrity of the BBB, resulting in leakiness, even though all glioblastomas may have clinically significant regions with an intact BBB [183]. These immuno-PET tracers could be informative to determine the grade of the BBB integrity of the tumor and could guide therapeutic interventions. The

clinical realities of the contribution of the BBB to treatment failure in glioblastoma argue for renewed efforts to develop BBB-penetrating immuno-PET tracers.

The development of immuno-PET probes based on antibody subunits targeting glioblastoma biomarkers can overcome BBB selectivity emerging as promising probes for the non-invasive diagnosis of gliomas [131]. Among them, sdAbs such as nanobodies present multiple properties, including a smaller MW, enabling better BBB entrance, tumor uptake and biodistribution, and faster clearance than conventional antibodies [132,133].

Various molecular mechanisms for the transportation of nanobodies through the Blood–Brain Barrier (BBB) have been extensively described and include adsorptive and receptor-mediated transcytosis, somatic gene transfer, and the use of carriers or shuttles such as cell-penetrating peptides, extracellular vesicles, liposomes, and nanoparticles as well as device-based and physicochemical disruption of the BBB [143–146].

The development of nanobody-based radiotracers for the non-invasive diagnosis of glioblastoma by immuno-PET may also involve some potential challenges. First, suboptimal imaging of glioblastoma may be achieved due to the low penetration of nanobodies through the BBB [184], although some nanobodies have shown their potential to access the brain parenchyma [143]. Second, the administration of nanobodies with theragnostic potential may elicit immunogenic responses. The immunogenicity risk profile of nanobodies with potential clinical applications is being evaluated [185] and further humanization of the structure of nanobodies by genetic engineering techniques will minimize the activation of the immune system [72,73]. The administration of nanobodies may also lead to potential renal toxicity due to the high kidney uptake of nanobodies [186]. To solve this issue, several approaches have been developed to decrease renal uptake of nanobodies without inducing additional side effects: *in vivo* pretreatment with biomolecules (e.g., sodium maleate or fructose) [187] and PEGylation of nanobodies [188,189].

Furthermore, the production of nanobodies in the current good-manufacturing-practice (cGMP) grade is essential for their application in clinics. cGMP includes meeting preclinical quality standards, validating the nanobody format without tags utilized for production [190] and the site-specific radiolabeling of nanobodies, increasing the cost and time of their production [191,192]. Further improvement of image reconstruction and multimodal imaging approaches based on nanobodies will pave the way for a more precise diagnosis of glioblastoma by immuno-PET techniques.

Recently, a bivalent nanobody for the treatment of patients suffering from thrombotic thrombocytopenic purpura (Caplacizumab, ALX-0681) [168,169] received approval from the FDA and the EMA, representing a cornerstone for domain antibodies in the clinic and giving this area of research a boost. Nanobodies can be labeled with PET isotopes of shorter half-lives, such as ^{68}Ga or ^{44}Sc , which can be produced in a generator [79–81], making immuno-PET more accessible and affordable.

In contrast to a reduction in tumor size as observed in MRI, which usually represents late treatment effects, biomarker changes can occur earlier. Immuno-PET allows the quantification of biomarkers in a non-invasive manner in the whole body and holds the potential of detecting functional glioblastoma biomarker changes helping to an earlier diagnosis of glioblastoma, surveillance of patients, and monitoring of treatment response.

8. Conclusions

The current diagnosis of glioblastoma by MRI in some situations does not allow proper discrimination of the tumoral tissue from concurrent processes and can be confounding with other lesions and post-therapeutic effects [3].

Immuno-PET represents an attractive and innovative option for diagnosing gliomas, allowing the analysis of biomarkers in a non-invasive manner. By merging the target selectivity and specificity of antibodies and derivatives toward a biomarker with the high sensitivity, spatial resolution, and quantitative capabilities of PET [178], allowing the quantification of biomarkers in a non-invasive manner in the whole body.

To date, several immuno-PET imaging tracers have been designed to target glioblastoma and have already proven successful in detecting gliomas in multiple preclinical models, and they are advancing through clinical trials. The development of immuno-PET probes based on antibodies and nanobodies can overcome BBB selectivity emerging as promising probes for the non-invasive diagnosis, surveillance of patients, and monitoring of treatment response of gliomas [131].

Author Contributions: Conceptualization, E.R.-L. and A.J.S.; investigation, E.R.-L., I.C.-Y., J.C.-P., M.J.G.-P., N.M.-C., M.Á.M. and A.J.S.; writing—original draft preparation, E.R.-L., J.C.-P., I.C.-Y., M.J.G.-P., N.M.-C., M.Á.M. and A.J.S.; writing—review and editing, supervision and funding acquisition, J.C.-P., M.Á.M. and A.J.S. All authors have read and agreed to the published version of the manuscript.

Funding: This research was funded by Instituto de Salud Carlos III through the Fondo de Investigación en Salud Project “PI18/01665” and co-funded by European Union (ERDF, “A way to make Europe”), the XIII Beca FERO en Investigación Oncológica Traslacional from Fundación FERO, Ayudas a la investigación del cáncer infantil from Asociación de Padres de Niños con Cáncer de Aragón (ASPANOA) (A.J.S.). Ayuda Predoctoral-Aragón from Asociación Española Contra el Cáncer (AECC) and Fundación Científica AECC (References.: PRDAR17002RUIZ for E.R.-L. and PRDAR18006MEND for N.M.-C. Ayudas para la Formación de Profesorado Universitario (FPU) from Ministerio de Universidades (FPU19/06371) (I.C.-Y.).

Institutional Review Board Statement: All image scans were obtained from our Center dataset, performed for clinical purposes using routine techniques, properly anonymized and an ethical review board approved written informed consent was obtained at the time of original clinical images collection. Thus, ethical review and approval were waived for this review article. The experimental animal procedures were conducted according to the guidelines and approved by the Competent Authority of the Regional Government of Madrid (CAM), Spain (projects PROEX 104/16 and PROEX 094/15) and they were performed in accordance with the guidelines stated in the International Guiding Principles for Biomedical Research Involving Animals, developed by the Council for International Organizations of Medical Sciences (CIOMS).

Acknowledgments: A.J.S. and E.R.-L. thank the Molecular Oncology Lab members at IIS Aragón for their critical reading of the manuscript. This review honors the memory of Michel Vallés and Nacho Bon Romero, who keep inspiring our work in the laboratory.

Conflicts of Interest: The authors declare no conflict of interest.

References

1. Ostrom, Q.T.; Cioffi, G.; Waite, K.; Kruchko, C.; Barnholtz-Sloan, J.S. CBTRUS Statistical Report: Primary Brain and Other Central Nervous System Tumors Diagnosed in the United States in 2014–2018. *Neuro-Oncology* **2021**, *23*, iii1–iii105. [[CrossRef](#)] [[PubMed](#)]
2. Wen, P.Y.; Santosh, K. Malignant gliomas in adults. *N. Engl. J. Med.* **2008**, *359*, 492–507. [[CrossRef](#)]
3. Ahmed, R.; Oborski, M.J.; Hwang, M.; Lieberman, F.S.; Mountz, J.M. Malignant gliomas: Current perspectives in diagnosis, treatment, and early response assessment using advanced quantitative imaging methods. *Cancer Manag. Res.* **2014**, *6*, 149–170. [[CrossRef](#)] [[PubMed](#)]
4. Verhaak, R.G.W.; Hoadley, K.A.; Purdom, E.; Wang, V.; Qi, Y.; Wilkerson, M.D.; Miller, C.R.; Ding, L.; Golub, T.; Mesirov, J.P.; et al. Integrated Genomic Analysis Identifies Clinically Relevant Subtypes of Glioblastoma Characterized by Abnormalities in PDGFRA, IDH1, EGFR, and NF1. *Cancer Cell* **2010**, *17*, 98–110. [[CrossRef](#)]
5. Deb, P.; Sharma, M.C.; Mahapatra, A.K.; Agarwal, D.; Sarkar, C. Glioblastoma multiforme with long term survival. *Neurol. India* **2005**, *53*, 329–332.
6. Henriksson, R.; Asklund, T.; Poulsen, H.S. Impact of therapy on quality of life, neurocognitive function and their correlates in glioblastoma multiforme: A review. *J. Neurooncol.* **2011**, *104*, 639–646. [[CrossRef](#)] [[PubMed](#)]
7. Stupp, R.; Hegi, M.E.; Mason, W.P.; van den Bent, M.J.; Taphoorn, M.J.; Janzer, R.C.; Ludwin, S.K.; Allgeier, A.; Fisher, B.; Belanger, K.; et al. Effects of radiotherapy with concomitant and adjuvant temozolomide versus radiotherapy alone on survival in glioblastoma in a randomised phase III study: 5-year analysis of the EORTC-NCIC trial. *Lancet Oncol.* **2009**, *10*, 459–466. [[CrossRef](#)]
8. Esteller, M.; Garcia-Foncillas, J.; Andion, E.; Goodman, S.N.; Hidalgo, O.F.; Vanaclocha, V.; Baylin, S.B.; Herman, J.G. Inactivation of the DNA-Repair Gene MGMT and the Clinical Response of Gliomas to Alkylating Agents. *N. Engl. J. Med.* **2000**, *349*, 1350–1354. [[CrossRef](#)]

9. Gilbert, M.R.; Wang, M.; Aldape, K.D.; Stupp, R.; Hegi, M.E.; Jaeckle, K.A.; Armstrong, T.S.; Wefel, J.S.; Won, M.; Blumenthal, D.T.; et al. Dose-dense temozolomide for newly diagnosed glioblastoma: A randomized phase III clinical trial. *J. Clin. Oncol.* **2013**, *31*, 4085–4091. [[CrossRef](#)]
10. FDA Approves Expanded Indication for Medical Device to Treat Glioblastoma Multiforme | ESMO. Available online: <https://www.esmo.org/oncology-news/archive/fda-approves-expanded-indication-for-medical-device-to-treat-glioblastoma-multiforme> (accessed on 11 August 2021).
11. Fabian, D.; Eibl, M.d.P.G.P.; Alnahhas, I.; Sebastian, N.; Giglio, P.; Puduvalli, V.; Gonzalez, J.; Palmer, J.D. Treatment of glioblastoma (GBM) with the addition of tumor-treating fields (TTF): A review. *Cancers* **2019**, *11*, 174. [[CrossRef](#)]
12. Louis, D.N.; Perry, A.; Reifenberger, G.; von Deimling, A.; Figarella-Branger, D.; Cavenee, W.K.; Ohgaki, H.; Wiestler, O.D.; Kleihues, P.; Ellison, D.W. The 2016 World Health Organization Classification of Tumors of the Central Nervous System: A summary. *Acta Neuropathol.* **2016**, *131*, 803–820. [[CrossRef](#)]
13. Reifenberger, G.; Wirsching, H.G.; Knobbe-Thomsen, C.B.; Weller, M. Advances in the molecular genetics of gliomas-implications for classification and therapy. *Nat. Rev. Clin. Oncol.* **2017**, *14*, 434–452. [[CrossRef](#)] [[PubMed](#)]
14. Louis, D.N.; Perry, A.; Wesseling, P.; Brat, D.J.; Cree, I.A.; Figarella-branger, D.; Hawkins, C.; Ng, H.K.; Pfister, S.M.; Reifenberger, G.; et al. The 2021 WHO Classification of Tumors of the Central Nervous System: A summary. *Neuro-Oncology* **2021**, *23*, 1215–1217. [[CrossRef](#)]
15. Capper, D.; Jones, D.T.W.; Sill, M.; Hovestadt, V.; Schrimpf, D.; Sturm, D.; Koelsche, C.; Sahm, F.; Chavez, L.; Reuss, D.E.; et al. DNA methylation-based classification of central nervous system tumours. *Nature* **2018**, *555*, 469–474. [[CrossRef](#)] [[PubMed](#)]
16. Brat, D.J.; Aldape, K.; Colman, H.; Holland, E.C.; Louis, D.N.; Jenkins, R.B.; Kleinschmidt-DeMasters, B.K.; Perry, A.; Reifenberger, G.; Stupp, R.; et al. cIMPACT-NOW update 3: Recommended diagnostic criteria for “Diffuse astrocytic glioma, IDH-wildtype, with molecular features of glioblastoma, WHO grade IV”. *Acta Neuropathol.* **2018**, *136*, 805–810. [[CrossRef](#)]
17. Tesileanu, C.M.S.; Dirven, L.; Wijnenga, M.M.J.; Koekkoek, J.A.F.; Vincent, A.J.P.E.; Dubbink, H.J.; Atmodimedjo, P.N.; Kros, J.M.; Van Duinen, S.G.; Smits, M.; et al. Survival of diffuse astrocytic glioma, IDH1/2 wildtype, with molecular features of glioblastoma, WHO grade IV: A confirmation of the cIMPACT-NOW criteria. *Neuro-Oncology* **2020**, *22*, 515–523. [[CrossRef](#)] [[PubMed](#)]
18. Lundy, P.; Domino, J.; Ryken, T.; Fouke, S.; McCracken, D.J.; Ormond, D.R.; Olson, J.J. The role of imaging for the management of newly diagnosed glioblastoma in adults: A systematic review and evidence-based clinical practice guideline update. *J. Neurooncol.* **2020**, *150*, 95–120. [[CrossRef](#)]
19. Castillo, M. History and evolution of brain tumor imaging: Insights through radiology. *Radiology* **2014**, *273*, S111–S125. [[CrossRef](#)]
20. Jain, R. Perfusion CT imaging of brain tumors: An overview. *Am. J. Neuroradiol.* **2011**, *32*, 1570–1577. [[CrossRef](#)]
21. Kerr, P.B.; Caputy, A.J.; Horwitz, N.H. A history of cerebral localization. *Neurosurg. Focus* **2005**, *18*, E1. [[CrossRef](#)]
22. Yao, J.; Chakhoyan, A.; Nathanson, D.A.; Yong, W.H.; Salamon, N.; Raymond, C.; Mareninov, S.; Lai, A.; Nghiemphu, P.L.; Prins, R.M.; et al. Metabolic characterization of human IDH mutant and wild type gliomas using simultaneous pH- and oxygen-sensitive molecular MRI. *Neuro-Oncology* **2019**, *21*, 1184–1196. [[CrossRef](#)] [[PubMed](#)]
23. Trinh, A.; Wintermark, M.; Iv, M. Clinical Review of Computed Tomography and MR Perfusion Imaging in Neuro-Oncology. *Radiol. Clin. N. Am.* **2021**, *59*, 323–334. [[CrossRef](#)]
24. Parker, N.R.; Khong, P.; Parkinson, J.F.; Howell, V.M.; Wheeler, H.R. Molecular heterogeneity in glioblastoma: Potential clinical implications. *Front. Oncol.* **2015**, *5*, 55. [[CrossRef](#)] [[PubMed](#)]
25. Weil, S.; Osswald, M.; Solecki, G.; Grosch, J.; Jung, E.; Lemke, D.; Ratliff, M.; Hänggi, D.; Wick, W.; Winkler, F. Tumor microtubes convey resistance to surgical lesions and chemotherapy in gliomas. *Neuro-Oncology* **2017**, *19*, 1316–1326. [[CrossRef](#)]
26. Petrecca, K.; Guiot, M.C.; Panet-Raymond, V.; Souhami, L. Failure pattern following complete resection plus radiotherapy and temozolomide is at the resection margin in patients with glioblastoma. *J. Neurooncol.* **2013**, *111*, 19–23. [[CrossRef](#)] [[PubMed](#)]
27. Drake, L.R.; Hillmer, A.T.; Cai, Z. Approaches to PET Imaging of Glioblastoma. *Molecules* **2020**, *25*, 568. [[CrossRef](#)]
28. Hillner, B.E.; Siegel, B.A.; Hanna, L.; Shields, A.F.; Duan, F.; Gareen, I.F.; Quinn, B.; Coleman, R.E. Impact of 18F-FDG PET used after initial treatment of cancer: Comparison of the national oncologic PET registry 2006 and 2009 cohorts. *J. Nucl. Med.* **2012**, *53*, 831–837. [[CrossRef](#)]
29. Hanahan, D.; Weinberg, R.A. Hallmarks of cancer: The next generation. *Cell* **2011**, *144*, 646–674. [[CrossRef](#)]
30. Som, P.; Atkins, H.L.; Bandyopadhyay, D.; Fowler, J.S.; MacGregor, R.R.; Matsui, K.; Oster, Z.H.; Sacker, D.F.; Shiue, C.Y.; Turner, H.; et al. A fluorinated glucose analog, 2-fluoro-2-deoxy-D-glucose (F-18). *J. Comput. Assist. Tomogr.* **1980**, *4*, 878. [[CrossRef](#)]
31. Lopci, E.; Fanti, S. Non-FDG PET/CT. *Recent Results Cancer Res.* **2020**, *216*, 669–718. [[CrossRef](#)]
32. Treglia, G.; Muoio, B.; Trevisi, G.; Mattoli, M.V.; Albano, D.; Bertagna, F.; Giovanella, L. Diagnostic Performance and Prognostic Value of PET/CT with Different Tracers for Brain Tumors: A Systematic Review of Published Meta-Analyses. *Int. J. Mol. Sci.* **2019**, *20*, 4669. [[CrossRef](#)] [[PubMed](#)]
33. Herminghaus, S.; Pilatus, U.; Möller-Hartmann, W.; Raab, P.; Lanfermann, H.; Schlote, W.; Zanella, F.E. Increased choline levels coincide with enhanced proliferative activity of human neuroepithelial brain tumors. *NMR Biomed.* **2002**, *15*, 385–392. [[CrossRef](#)] [[PubMed](#)]
34. Treglia, G.; Giovannini, E.; Di Franco, D.; Calcagni, M.L.; Rufini, V.; Picchio, M.; Giordano, A. The role of positron emission tomography using carbon-11 and fluorine-18 choline in tumors other than prostate cancer: A systematic review. *Ann. Nucl. Med.* **2012**, *26*, 451–461. [[CrossRef](#)] [[PubMed](#)]

35. Gao, L.; Xu, W.; Li, T.; Zheng, J.; Chen, G. Accuracy of 11C-choline positron emission tomography in differentiating glioma recurrence from radiation necrosis: A systematic review and meta-analysis. *Medicine* **2018**, *97*, e11556. [[CrossRef](#)] [[PubMed](#)]
36. Alongi, P.; Vetrano, I.G.; Fiasconaro, E.; Alaimo, V.; Laudicella, R.; Bellavia, M.; Rubino, F.; Bagnato, S.; Galardi, G. Choline-PET/CT in the Differential Diagnosis Between Cystic Glioblastoma and Intraparenchymal Hemorrhage. *Curr. Radiopharm.* **2019**, *12*, 88–92. [[CrossRef](#)] [[PubMed](#)]
37. La Fougère, C.; Suchorska, B.; Bartenstein, P.; Kreth, F.W.; Tonn, J.C. Molecular imaging of gliomas with PET: Opportunities and limitations. *Neuro-Oncology* **2011**, *13*, 806–819. [[CrossRef](#)] [[PubMed](#)]
38. Kläsner, B.D.; Krause, B.J.; Beer, A.J.; Drzezga, A. PET imaging of gliomas using novel tracers: A sleeping beauty waiting to be kissed. *Expert Rev. Anticancer Ther.* **2010**, *10*, 609–613. [[CrossRef](#)]
39. Laudicella, R.; Quartuccio, N.; Argiroffi, G.; Alongi, P.; Baratto, L.; Califaretti, E.; Frantellizzi, V.; De Vincentis, G.; Del Sole, A.; Evangelista, L.; et al. Unconventional non-amino acidic PET radiotracers for molecular imaging in gliomas. *Eur. J. Nucl. Med. Mol. Imaging* **2021**, *48*, 3925–3939. [[CrossRef](#)]
40. Horsman, M.R.; Mortensen, L.S.; Petersen, J.B.; Busk, M.; Overgaard, J. Imaging hypoxia to improve radiotherapy outcome. *Nat. Rev. Clin. Oncol.* **2012**, *9*, 674–687. [[CrossRef](#)]
41. Bell, C.; Dowson, N.; Fay, M.; Thomas, P.; Puttick, S.; Gal, Y.; Rose, S. Hypoxia imaging in gliomas with 18F-fluoromisonidazole PET: Toward clinical translation. *Semin. Nucl. Med.* **2015**, *45*, 136–150. [[CrossRef](#)]
42. Valk, P.E.; Mathis, C.A.; Prados, M.D.; Gilbert, J.C.; Budinger, T.F. Hypoxia in human gliomas: Demonstration by PET with fluorine-18- fluoromisonidazole. *J. Nucl. Med.* **1992**, *33*, 2133–2137. [[PubMed](#)]
43. Challapalli, A.; Carroll, L.; Aboagye, E.O. Molecular mechanisms of hypoxia in cancer. *Clin. Transl. Imaging* **2017**, *5*, 225–253. [[CrossRef](#)]
44. Roncaroli, F.; Su, Z.; Herholz, K.; Gerhard, A.; Turkheimer, F.E. TSPO expression in brain tumours: Is TSPO a target for brain tumour imaging? *Clin. Transl. Imaging* **2016**, *4*, 145–156. [[CrossRef](#)]
45. Werner, J.M.; Lohmann, P.; Fink, G.R.; Langen, K.J.; Galldiks, N. Current landscape and emerging fields of PET imaging in patients with brain tumors. *Molecules* **2020**, *25*, 1471. [[CrossRef](#)] [[PubMed](#)]
46. Freise, A.C.; Wu, A.M. In vivo imaging with antibodies and engineered fragments. *Mol. Immunol.* **2015**, *67*, 142–152. [[CrossRef](#)]
47. van Dongen, G.A.M.S.; Visser, G.W.M.; Lub-de Hooge, M.N.; de Vries, E.G.; Perk, L.R. Immuno-PET: A Navigator in Monoclonal Antibody Development and Applications. *Oncologist* **2007**, *12*, 1379–1389. [[CrossRef](#)] [[PubMed](#)]
48. Pandit-Taskar, N.; Postow, M.A.; Hellmann, M.D.; Harding, J.J.; Barker, C.A.; O'Donoghue, J.A.; Ziolkowska, M.; Ruan, S.; Lyashchenko, S.K.; Tsai, F.; et al. First-in-Humans Imaging with 89Zr-Df-IAB22M2C Anti-CD8 Minibody in Patients with Solid Malignancies: Preliminary Pharmacokinetics, Biodistribution, and Lesion Targeting. *J. Nucl. Med.* **2020**, *61*, 512–519. [[CrossRef](#)]
49. Wu, A.M. Engineered antibodies for molecular imaging of cancer. *Methods* **2014**, *65*, 139–147. [[CrossRef](#)]
50. Kim, H.; Kim, Y.M. Pan-cancer analysis of somatic mutations and transcriptomes reveals common functional gene clusters shared by multiple cancer types. *Sci. Rep.* **2018**, *8*, 6041. [[CrossRef](#)]
51. Chakraborty, S.; Hosen, M.I.; Ahmed, M.; Shekhar, H.U. Onco-Multi-OMICS Approach: A New Frontier in Cancer Research. *BioMed Res. Int.* **2018**, *2018*, 9836256. [[CrossRef](#)]
52. Keizer, R.J.; Huitema, A.D.R.; Schellens, J.H.M.; Beijnen, J.H. Clinical pharmacokinetics of therapeutic monoclonal antibodies. *Clin. Pharmacokinet.* **2010**, *49*, 493–507. [[CrossRef](#)]
53. James, M.L.; Gambhir, S.S. A molecular imaging primer: Modalities, imaging agents, and applications. *Physiol. Rev.* **2012**, *92*, 897–965. [[CrossRef](#)]
54. Knowles, S.M.; Wu, A.M. Advances in immuno-positron emission tomography: Antibodies for molecular imaging in oncology. *J. Clin. Oncol.* **2012**, *30*, 3884–3892. [[CrossRef](#)]
55. Heskamp, S.; Van Laarhoven, H.W.M.; Molkenboer-Kuening, J.D.M.; Bouwman, W.H.; Van Der Graaf, W.T.A.; Oyen, W.J.G.; Boerman, O.C. Optimization of IGF-1R SPECT/CT imaging using 111In-labeled F(ab)₂ and Fab fragments of the monoclonal antibody R1507. *Mol. Pharm.* **2012**, *9*, 2314–2321. [[CrossRef](#)] [[PubMed](#)]
56. Lütje, S.; van Rij, C.M.; Franssen, G.M.; Fracasso, G.; Helfrich, W.; Eek, A.; Oyen, W.J.; Colombatti, M.; Boerman, O.C. Targeting human prostate cancer with 111In-labeled D2B IgG, F(ab')₂ and Fab fragments in nude mice with PSMA-expressing xenografts. *Contrast Media Mol. Imaging* **2015**, *10*, 28–36. [[CrossRef](#)] [[PubMed](#)]
57. Kerdjoudj, R.; Pniok, M.; Alliot, C.; Kubíček, V.; Havlíčková, J.; Rösch, F.; Hermann, P.; Huclier-Markai, S. Scandium(III) complexes of monophosphorus acid DOTA analogues: A thermodynamic and radiolabelling study with 44Sc from cyclotron and from a 44Ti/44Sc generator. *Dalt. Trans.* **2016**, *45*, 1398–1409. [[CrossRef](#)]
58. Romero, E.; Martínez, A.; Oteo, M.; Ibañez, M.; Santos, M.; Morcillo, M.Á. Development and long-term evaluation of a new 68Ge/68Ga generator based on nano-SnO₂ for PET imaging. *Sci. Rep.* **2020**, *10*, 12756. [[CrossRef](#)] [[PubMed](#)]
59. González-Gómez, R.; Pazo-Cid, R.A.; Sarria, L.; Morcillo, M.Á.; Schuhmacher, A.J. Diagnosis of Pancreatic Ductal Adenocarcinoma by Immuno-Positron Emission Tomography. *J. Clin. Med.* **2021**, *10*, 1151. [[CrossRef](#)]
60. De Aguiar, R.B.; da Silva, T.d.A.; Costa, B.A.; Machado, M.F.M.; Yamada, R.Y.; Braggion, C.; Perez, K.R.; Mori, M.A.S.; Oliveira, V.; de Moraes, J.Z. Generation and functional characterization of a single-chain variable fragment (scFv) of the anti-FGF2 3F12E7 monoclonal antibody. *Sci. Rep.* **2021**, *11*, 1432. [[CrossRef](#)]
61. Van Tellingen, O.; Yetkin-Arik, B.; De Gooijer, M.C.; Wesseling, P.; Wurdinger, T.; De Vries, H.E. Overcoming the blood-brain tumor barrier for effective glioblastoma treatment. *Drug Resist. Updat.* **2015**, *19*, 1–12. [[CrossRef](#)]

62. Poli, G.L.; Bianchi, C.; Virota, G.; Bettini, A.; Moretti, R.; Trachsel, E.; Elia, G.; Giovannoni, L.; Neri, D.; Bruno, A. Radretumab radioimmunotherapy in patients with brain metastasis: A 124I-L19SIP dosimetric PET study. *Cancer Immunol. Res.* **2013**, *1*, 134–143. [[CrossRef](#)]
63. Muyltermans, S.; Baral, T.N.; Retamozzo, V.C.; De Baetselier, P.; De Genst, E.; Kinne, J.; Leonhardt, H.; Magez, S.; Nguyen, V.K.; Revets, H.; et al. Camelid immunoglobulins and nanobody technology. *Vet. Immunol. Immunopathol.* **2009**, *128*, 178–183. [[CrossRef](#)]
64. Nuttall, S.D. Overview and discovery of IgNARs and generation of VNARs. *Methods Mol. Biol.* **2012**, *911*, 27–36. [[CrossRef](#)]
65. Abskharon, R.N.N.; Giachin, G.; Wohlkonig, A.; Soror, S.H.; Pardon, E.; Legname, G.; Steyaert, J. Probing the N-terminal β -sheet conversion in the crystal structure of the human prion protein bound to a nanobody. *J. Am. Chem. Soc.* **2014**, *136*, 937–944. [[CrossRef](#)]
66. Staus, D.P.; Wingler, L.M.; Strachan, R.T.; Rasmussen, S.G.F.; Pardon, E.; Ahn, S.; Steyaert, J.; Kobilka, B.K.; Lefkowitz, R.J. Regulation of b2-Adrenergic Receptor Function by Conformationally Selective Single-Domain Intrabodies. *Mol. Pharmacol.* **2014**, *85*, 472–481. [[CrossRef](#)] [[PubMed](#)]
67. De Genst, E.; Silence, K.; Decanniere, K.; Conrath, K.; Loris, R.; Kinne, J.; Muyltermans, S.; Wyns, L. Molecular basis for the preferential cleft recognition by dromedary heavy-chain antibodies. *Proc. Natl. Acad. Sci. USA* **2006**, *103*, 4586–4591. [[CrossRef](#)] [[PubMed](#)]
68. Ren, G.; Zhang, R.; Liu, Z.; Webster, J.M.; Miao, Z.; Gambhir, S.S.; Syud, F.A.; Cheng, Z. A 2-helix small protein labeled with 68Ga for PET imaging of HER2 expression. *J. Nucl. Med.* **2009**, *50*, 1492–1499. [[CrossRef](#)]
69. Atkins, K.L.; Burman, J.D.; Chamberlain, E.S.; Cooper, J.E.; Poutrel, B.; Bagby, S.; Jenkins, A.T.A.; Feil, E.J.; van den Elsen, J.M.H. *S. aureus* IgG-binding proteins SpA and Sbi: Host specificity and mechanisms of immune complex formation. *Mol. Immunol.* **2008**, *45*, 1600–1611. [[CrossRef](#)] [[PubMed](#)]
70. Schoonoghe, S.; Laoui, D.; Van Ginderachter, J.A.; Devoogdt, N.; Lahoutte, T.; De Baetselier, P.; Raes, G. Novel applications of nanobodies for in vivo bio-imaging of inflamed tissues in inflammatory diseases and cancer. *Immunobiology* **2012**, *217*, 1266–1272. [[CrossRef](#)] [[PubMed](#)]
71. Almagro, J.C.; Fransson, J. Humanization of antibodies. *Front. Biosci.* **2008**, *13*, 1619–1633. [[CrossRef](#)] [[PubMed](#)]
72. Soler, M.A.; Medagli, B.; Wang, J.; Oloketuyi, S.; Bajc, G.; Huang, H.; Fortuna, S.; De Marco, A. Effect of humanizing mutations on the stability of the llama single-domain variable region. *Biomolecules* **2021**, *11*, 163. [[CrossRef](#)]
73. Rossotti, M.A.; Bélanger, K.; Henry, K.A.; Tanha, J. Immunogenicity and humanization of single-domain antibodies. *FEBS J.* **2021**, *2021*, 1–24. [[CrossRef](#)] [[PubMed](#)]
74. Smith, D.L.; Breeman, W.A.P.; Sims-Mourtada, J. The untapped potential of Gallium 68-PET: The next wave of 68Ga-agents. *Appl. Radiat. Isot.* **2013**, *76*, 14–23. [[CrossRef](#)]
75. Rodnick, M.E.; Sollert, C.; Stark, D.; Clark, M.; Katsifis, A.; Hockley, B.G.; Parr, D.C.; Frigell, J.; Henderson, B.D.; Abghari-Gerst, M.; et al. Cyclotron-based production of 68Ga, [68Ga]GaCl₃, and [68Ga]Ga-PSMA-11 from a liquid target. *EJNMMI Radiopharm. Chem.* **2020**, *5*, 25. [[CrossRef](#)]
76. Thisgaard, H.; Kumlin, J.; Langkjær, N.; Chua, J.; Hook, B.; Jensen, M.; Kassaian, A.; Zeisler, S.; Borjjan, S.; Cross, M.; et al. Multi-curie production of gallium-68 on a biomedical cyclotron and automated radiolabelling of PSMA-11 and DOTATATE. *EJNMMI Radiopharm. Chem.* **2021**, *6*, 1. [[CrossRef](#)] [[PubMed](#)]
77. van der Meulen, N.P.; Hasler, R.; Talip, Z.; Grundler, P.V.; Favaretto, C.; Umbricht, C.A.; Müller, C.; Dellepiane, G.; Carzaniga, T.S.; Braccini, S. Developments toward the implementation of 44Sc production at a medical cyclotron. *Molecules* **2020**, *25*, 4706. [[CrossRef](#)] [[PubMed](#)]
78. Lowis, C.; Ferguson, S.; Paulßen, E.; Hoehr, C. Improved Sc-44 production in a siphon-style liquid target on a medical cyclotron. *Appl. Radiat. Isot.* **2021**, *172*, 109675. [[CrossRef](#)] [[PubMed](#)]
79. Romero, E.; Morcillo, M.A. Inorganic oxides with potential application in the preparation of a 68Ge/68Ga generator system. *Appl. Radiat. Isot.* **2017**, *119*, 28–35. [[CrossRef](#)] [[PubMed](#)]
80. Rosar, F.; Buchholz, H.G.; Michels, S.; Hoffmann, M.A.; Piel, M.; Waldmann, C.M.; Rösch, F.; Reuss, S.; Schreckenberger, M. Image quality analysis of 44Sc on two preclinical PET scanners: A comparison to 68Ga. *EJNMMI Phys.* **2020**, *7*, 16. [[CrossRef](#)]
81. Rosar, F.; Bohnenberger, H.; Moon, E.S.; Rösch, F.; Denig, A.; Vincenz-Zörner, D.; Hoffmann, M.A.; Khreish, F.; Ezziddin, S.; Schreckenberger, M.; et al. Impact of prompt gamma emission of 44Sc on quantification in preclinical and clinical PET systems. *Appl. Radiat. Isot.* **2021**, *170*, 109599. [[CrossRef](#)]
82. Cal-González, J.; Lage, E.; Herranz, E.; Vicente, E.; Udias, J.M.; Moore, S.C.; Park, M.; Dave, S.R.; Parot, V.; Herraiz, J.L. Simulation of triple coincidences in PET. *Phys. Med. Biol.* **2015**, *60*, 117–136. [[CrossRef](#)]
83. Sutherland, A. Radiohalogenation of Organic Compounds: Practical Considerations and Challenges for Molecular Imaging. *Synthesis* **2019**, *51*, 4368–4373. [[CrossRef](#)]
84. Deri, M.A.; Ponnala, S.; Zeglis, B.M.; Pohl, G.; Dannenberg, J.J.; Lewis, J.S.; Francesconi, L.C. Alternative Chelator for 89Zr Radiopharmaceuticals: Radiolabeling and Evaluation of 3,4,3-(LI-1,2-HOPO). *J. Med. Chem.* **2014**, *57*, 4849–4860. [[CrossRef](#)] [[PubMed](#)]
85. Tsionou, M.I.; Knapp, C.E.; Foley, C.A.; Munteanu, C.R.; Cakebread, A.; Imberti, C.; Eykyn, T.R.; Young, J.D.; Paterson, B.M.; Blower, J.; et al. Comparison of macrocyclic and acyclic chelators for gallium-68 radiolabelling. *RSC Adv.* **2017**, *7*, 49586–49599. [[CrossRef](#)] [[PubMed](#)]

86. Romero, E.; Martínez, A.; Oteo, M.; García, A.; Morcillo, M.A. Preparation of ⁶⁸Ga-labelled DOTA-peptides using a manual labelling approach for small-animal PET imaging. *Appl. Radiat. Isot.* **2016**, *107*, 113–120. [[CrossRef](#)]
87. Agarwal, P.; Bertozzi, C.R. Site-Specific Antibody–Drug Conjugates: The Nexus of Bioorthogonal Chemistry, Protein Engineering, and Drug Development. *Bioconjug. Chem.* **2015**, *26*, 176–192. [[CrossRef](#)] [[PubMed](#)]
88. Kolb, H.C.; Finn, M.G.; Sharpless, K.B. Click Chemistry: Diverse Chemical Function from a Few Good Reactions. *Angew. Chemie Int. Ed.* **2001**, *40*, 2004–2021. [[CrossRef](#)]
89. Devaraj, N.K. The Future of Bioorthogonal Chemistry. *ACS Cent. Sci.* **2018**, *4*, 952–959. [[CrossRef](#)]
90. Knight, J.C.; Cornelissen, B. Bioorthogonal chemistry: Implications for pretargeted nuclear (PET/SPECT) imaging and therapy. *Am. J. Nucl. Med. Mol. Imaging* **2014**, *4*, 96–113.
91. Evans, H.L.; Carroll, L.S.; Kaliszczak, M.; Twyman, F.J.; Spivey, A.C.; Aboagye, E.O. A bioorthogonal ⁶⁸Ga-labelling strategy for rapid in vivo imaging. *Chem. Commun.* **2014**, *50*, 9557–9560. [[CrossRef](#)]
92. Yang, L.; Mao, H.; Wang, Y.A.; Cao, Z.; Peng, X.; Wang, X.; Duan, H.; Ni, C.; Yuan, Q.; Adams, G.; et al. Single Chain Epidermal Growth Factor Receptor Antibody Conjugated Nanoparticles for in vivo Tumor Targeting and Imaging. *Small* **2009**, *98195*, 235–243. [[CrossRef](#)]
93. Wang, X.; Xing, X.; Zhang, B.; Liu, F.; Cheng, Y.; Shi, D. Surface engineered antifouling optomagnetic SPIONs for bimodal targeted imaging of pancreatic cancer cells. *Int. J. Nanomed.* **2014**, *9*, 1601–1615. [[CrossRef](#)] [[PubMed](#)]
94. Da Pieve, C.; Makarem, A.; Turnock, S.; Maczynska, J.; Smith, G.; Kramer-Marek, G. Thiol-reactive PODs-bearing bifunctional chelators for the development of EGFR-targeting [¹⁸F]AlF-affibody conjugates. *Molecules* **2020**, *25*, 1562. [[CrossRef](#)]
95. Lee, F.T.; Burvenich, I.J.G.; Guo, N.; Kocovski, P.; Tochon-Danguy, H.; Ackermann, U.; O’Keefe, G.J.; Gong, S.; Rigopoulos, A.; Liu, Z.; et al. l-Tyrosine Confers Residualizing Properties to a d-Amino Acid-Rich Residualizing Peptide for Radioiodination of Internalizing Antibodies. *Mol. Imaging* **2016**, *15*, 1536012116647535. [[CrossRef](#)] [[PubMed](#)]
96. Chakravarty, R.; Goel, S.; Valdovinos, H.F.; Hernandez, R.; Hong, H.; Nickles, R.J.; Cai, W. Matching the decay half-life with the biological half-life: ImmunPET imaging with ⁴⁴Sc-labeled Cetuximab Fab fragment. *Bioconjug. Chem.* **2014**, *25*, 2197–2204. [[CrossRef](#)]
97. Tran, V.L.; Novell, A.; Tournier, N.; Gerstenmayer, M.; Schweitzer-Chaput, A.; Mateos, C.; Jegou, B.; Bouleau, A.; Nozach, H.; Winkeler, A.; et al. Impact of blood-brain barrier permeabilization induced by ultrasound associated to microbubbles on the brain delivery and kinetics of cetuximab: An immunPET study using ⁸⁹Zr-cetuximab. *J. Control. Release* **2020**, *328*, 304–312. [[CrossRef](#)] [[PubMed](#)]
98. Luo, H.; Hernandez, R.; Hong, H.; Graves, S.A.; Yang, Y.; England, C.G.; Theuer, C.P.; Nickles, R.J.; Cai, W. Noninvasive brain cancer imaging with a bispecific antibody fragment, generated via click chemistry. *Proc. Natl. Acad. Sci. USA* **2015**, *112*, 12806–12811. [[CrossRef](#)]
99. Puttick, S.; Stringer, B.W.; Day, B.W.; Bruce, Z.C.; Ensbey, K.S.; Mardon, K.; Cowin, G.J.; Thurecht, K.J.; Whittaker, A.K.; Fay, M.; et al. EphA2 as a Diagnostic Imaging Target in Glioblastoma: A Positron Emission Tomography/Magnetic Resonance Imaging Study. *Mol. Imaging* **2015**, *14*, 385–395. [[CrossRef](#)]
100. Sheybani, N.D.; Breza, V.R.; Paul, S.; McCauley, K.S.; Berr, S.S.; Miller, G.W.; Neumann, K.D.; Price, R.J. ImmunPET-informed sequence for focused ultrasound-targeted mCD47 blockade controls glioma. *J. Control. Release* **2021**, *331*, 19–29. [[CrossRef](#)]
101. Gaedicke, S.; Braun, F.; Prasad, S.; Machein, M.; Firat, E.; Hettich, M.; Gudihal, R.; Zhu, X.; Klingner, K.; Schüler, J.; et al. Noninvasive positron emission tomography and fluorescence imaging of CD133+ tumor stem cells. *Proc. Natl. Acad. Sci. USA* **2014**, *111*, E692–E701. [[CrossRef](#)]
102. Lesniak, W.G.; Chu, C.; Jablonska, A.; Du, Y.; Pomper, M.G.; Walczak, P.; Janowski, M. A distinct advantage to intraarterial delivery of ⁸⁹Zr-bevacizumab in PET imaging of mice with and without osmotic opening of the blood–brain barrier. *J. Nucl. Med.* **2019**, *60*, 617–622. [[CrossRef](#)] [[PubMed](#)]
103. Liu, H.-L.; Hsu, P.-H.; Lin, C.-Y.; Huang, C.-W.; Chai, W.-Y.; Chu, P.-C.; Huang, C.-Y.; Chen, P.-Y.; Yang, L.-Y.; Kuo, J.S.; et al. Focused Ultrasound Enhances Central Nervous System Delivery of Bevacizumab for Malignant Glioma Treatment. *Radiology* **2016**, *281*, 99–108. [[CrossRef](#)]
104. Hernandez, R.; Sun, H.; England, C.G.; Valdovinos, H.F.; Barnhart, T.E.; Yang, Y.; Cai, W. ImmunPET imaging of CD146 expression in malignant brain tumors. *Mol. Pharm.* **2016**, *13*, 2563–2570. [[CrossRef](#)]
105. Yang, Y.; Hernandez, R.; Rao, J.; Yin, L.; Qu, Y.; Wu, J.; England, C.G.; Graves, S.A.; Lewis, C.M.; Wang, P.; et al. Targeting CD146 with a ⁶⁴Cu-labeled antibody enables in vivo immunPET imaging of high-grade gliomas. *Proc. Natl. Acad. Sci. USA* **2015**, *112*, E6525–E6534. [[CrossRef](#)] [[PubMed](#)]
106. Zhou, B.; Wang, H.; Liu, R.; Wang, M.; Deng, H.; Giglio, B.C.; Gill, P.S.; Shan, H.; Li, Z. PET Imaging of Dll4 expression in glioblastoma and colorectal cancer xenografts using ⁶⁴Cu-labeled monoclonal antibody 61B. *Mol. Pharm.* **2015**, *12*, 3527–3534. [[CrossRef](#)] [[PubMed](#)]
107. De Lucas, A.G.; Schuhmacher, A.J.; Oteo, M.; Romero, E.; Cámara, J.A.; de Martino, A.; Arroyo, A.G.; Morcillo, M.; Squatrito, M.; Martinez-Torrecuadrada, J.L.; et al. Targeting MT1-MMP as an immunPET-based strategy for imaging gliomas. *PLoS ONE* **2016**, *11*, e0158634. [[CrossRef](#)]

108. Gonzalez-Junca, A.; Reiners, O.; Borrero-Garcia, L.D.; Beckford-Vera, D.; Lazar, A.A.; Chou, W.; Braunstein, S.; VanBrocklin, H.; Franc, B.L.; Barcellos-Hoff, M.H. Positron Emission Tomography Imaging of Functional Transforming Growth Factor β (TGF β) Activity and Benefit of TGF β Inhibition in Irradiated Intracranial Tumors. *Int. J. Radiat. Oncol. Biol. Phys.* **2021**, *109*, 527–539. [[CrossRef](#)]
109. Den Hollander, M.W.; Bensch, F.; Glaudemans, A.W.J.M.; Oude Munnink, T.H.; Enting, R.H.; Den Dunnen, W.F.A.; Heesters, M.A.A.M.; Kruyt, F.A.E.; Lub-De Hooge, M.N.; De Groot, J.C.; et al. TGF- β antibody uptake in recurrent high-grade glioma imaged with ⁸⁹Zr-fresolimumab PET. *J. Nucl. Med.* **2015**, *56*, 1310–1314. [[CrossRef](#)]
110. Pandya, D.N.; Sinha, A.; Yuan, H.; Mutkus, L.; Stumpf, K.; Marini, F.C.; Wadas, T.J. Imaging of fibroblast activation protein alpha expression in a preclinical mouse model of glioma using positron emission tomography. *Molecules* **2020**, *25*, 3672. [[CrossRef](#)] [[PubMed](#)]
111. Molotkov, A.; Doubrovin, M.; Bhatt, N.; Hsu, F.C.; Beserra, A.; Chopra, R.; Mintz, A. 3D optical/CT as a preclinical companion imaging platform for glioblastoma drug development. *Drug Deliv.* **2020**, *27*, 1686–1694. [[CrossRef](#)]
112. Liu, Q.; Jiang, L.; Li, K.; Li, H.; Lv, G.; Lin, J.; Qiu, L. Immuno-PET imaging of ⁶⁸Ga-labeled nanobody Nb109 for dynamic monitoring the PD-L1 expression in cancers. *Cancer Immunol. Immunother.* **2021**, *70*, 1721–1733. [[CrossRef](#)]
113. Kasten, B.B.; Houson, H.A.; Coleman, J.M.; Leavenworth, J.W.; Markert, J.M.; Wu, A.M.; Salazar, F.; Tavaré, R.; Massicano, A.V.F.; Gillespie, G.Y.; et al. Positron emission tomography imaging with ⁸⁹Zr—Labeled anti—CD8 cys—Diabody reveals—Infiltration during oncolytic virus therapy in a glioma murine model. *Sci. Rep.* **2021**, *11*, 15384. [[CrossRef](#)]
114. Nigam, S.; McCarl, L.; Kumar, R.; Edinger, R.S.; Kurland, B.F.; Anderson, C.J.; Panigrahy, A.; Kohanbash, G.; Edwards, W.B. Preclinical ImmunoPET Imaging of Glioblastoma-Infiltrating Myeloid Cells Using Zirconium-89 Labeled Anti-CD11b Antibody. *Mol. Imaging Biol.* **2020**, *22*, 685–694. [[CrossRef](#)] [[PubMed](#)]
115. Foster, A.; Nigam, S.; Tatum, D.S.; Raphael, I.; Xu, J.; Kumar, R.; Plakseychuk, E.; Latoche, J.D.; Vincze, S.; Li, B.; et al. Novel theranostic agent for PET imaging and targeted radiopharmaceutical therapy of tumour-infiltrating immune cells in glioma. *EBioMedicine* **2021**, *71*, 103571. [[CrossRef](#)]
116. Nobashi, T.W.; Mayer, A.T.; Xiao, Z.; Chan, C.T.; Chaney, A.M.; James, M.L.; Gambhir, S.S. Whole-body PET imaging of T cell response to Glioblastoma. *Clin. Cancer Res.* **2021**, *27*, 6445–6456. [[CrossRef](#)] [[PubMed](#)]
117. Quail, D.F.; Joyce, J.A. The Microenvironmental Landscape of Brain Tumors. *Cancer Cell* **2017**, *31*, 326–341. [[CrossRef](#)] [[PubMed](#)]
118. Pyonteck, S.M.; Akkari, L.; Schuhmacher, A.J.; Bowman, R.L.; Sevenich, L.; Quail, D.F.; Olson, O.C.; Quick, M.L.; Huse, J.T.; Teijeiro, V.; et al. CSF-1R inhibition alters macrophage polarization and blocks glioma progression. *Nat. Med.* **2013**, *19*, 1264–1272. [[CrossRef](#)]
119. Quail, D.F.; Bowman, R.L.; Akkari, L.; Quick, M.L.; Schuhmacher, A.J.; Huse, J.T.; Holland, E.C.; Sutton, J.C.; Joyce, J.A. The tumor microenvironment underlies acquired resistance to CSF-1R inhibition in gliomas. *Science* **2016**, *352*, aad3018. [[CrossRef](#)]
120. Bouleau, A.; Lebon, V.; Truillet, C. PET imaging of immune checkpoint proteins in oncology. *Pharmacol. Ther.* **2021**, *222*, 107786. [[CrossRef](#)]
121. Lu, C.T.; Zhao, Y.Z.; Wong, H.L.; Cai, J.; Peng, L.; Tian, X.Q. Current approaches to enhance CNS delivery of drugs across the brain barriers. *Int. J. Nanomed.* **2014**, *9*, 2241–2257. [[CrossRef](#)]
122. Pardridge, W.M. Drug targeting to the brain. *Pharm. Res.* **2007**, *24*, 1733–1744. [[CrossRef](#)]
123. Dong, X. Current strategies for brain drug delivery. *Theranostics* **2018**, *8*, 1481–1493. [[CrossRef](#)] [[PubMed](#)]
124. Brasnjevic, I.; Steinbusch, H.W.M.; Schmitz, C.; Martinez-Martinez, P. Delivery of peptide and protein drugs over the blood-brain barrier. *Prog. Neurobiol.* **2009**, *87*, 212–251. [[CrossRef](#)]
125. Levites, Y.; Smithson, L.A.; Price, R.W.; Dakin, R.S.; Yuan, B.; Sierks, M.R.; Kim, J.; McGowan, E.; Kim Reed, D.; Rosenberry, T.L.; et al. Insights into the mechanisms of action of anti-A β antibodies in Alzheimer’s disease mouse models. *FASEB J.* **2006**, *20*, 2576–2578. [[CrossRef](#)] [[PubMed](#)]
126. Pepinsky, R.B.; Shao, Z.; Ji, B.; Wang, Q.; Meng, G.; Walus, L.; Lee, X.; Hu, Y.; Graff, C.; Garber, E.; et al. Exposure levels of anti-LINGO-1 Li81 antibody in the central nervous system and dose-efficacy relationships in rat spinal cord remyelination models after systemic administration. *J. Pharmacol. Exp. Ther.* **2011**, *339*, 519–529. [[CrossRef](#)] [[PubMed](#)]
127. Zhang, Y.; Pardridge, W.M. Rapid transferrin efflux from brain to blood across the blood-brain barrier. *J. Neurochem.* **2001**, *76*, 1597–1600. [[CrossRef](#)] [[PubMed](#)]
128. Siegelman, J.; Fleit, H.B.; Peress, N.S. Characterization of immunoglobulin G-Fc receptor activity in the outflow system of the cerebrospinal fluid. *Cell Tissue Res.* **1987**, *248*, 599–605. [[CrossRef](#)]
129. Cooper, P.R.; Ciambone, G.J.; Kliwinski, C.M.; Maze, E.; Johnson, L.; Li, Q.; Feng, Y.; Hornby, P.J. Efflux of monoclonal antibodies from rat brain by neonatal Fc receptor, FcRn. *Brain Res.* **2013**, *1534*, 13–21. [[CrossRef](#)]
130. Ruano-Salguero, J.S.; Lee, K.H. Antibody transcytosis across brain endothelial-like cells occurs nonspecifically and independent of FcRn. *Sci. Rep.* **2020**, *10*, 3685. [[CrossRef](#)]
131. Salvador, J.P.; Vilaplana, L.; Marco, M.P. Nanobody: Outstanding features for diagnostic and therapeutic applications. *Anal. Bioanal. Chem.* **2019**, *411*, 1703–1713. [[CrossRef](#)]
132. Krasniqi, A.; D’Huyvetter, M.; Devoogdt, N.; Frejd, F.Y.; Sörensen, J.; Orlova, A.; Keyaerts, M.; Tolmachev, V. Same-day imaging using small proteins: Clinical experience and translational prospects in oncology. *J. Nucl. Med.* **2018**, *59*, 885–891. [[CrossRef](#)]
133. Širochmanová, I.; Čomor, L.; Káňová, E.; Jiménez-Munguía, I.; Tkáčová, Z.; Bhide, M. Permeability of the Blood-Brain Barrier and Transport of Nanobodies Across the Blood-Brain Barrier. *Folia Vet.* **2018**, *62*, 59–66. [[CrossRef](#)]

134. Hamers-Casterman, C.; Atarhouch, T.; Muyldermans, S.; Robinson, G.; Hammers, C.; Songa, E.B.; Bendahman, N.; Hammers, R. Naturally occurring antibodies devoid of light chains. *Nature* **1993**, *363*, 446–448. [[CrossRef](#)] [[PubMed](#)]
135. Muyldermans, S. Nanobodies: Natural single-domain antibodies. *Annu. Rev. Biochem.* **2013**, *82*, 775–797. [[CrossRef](#)]
136. Jovčevska, I.; Muyldermans, S. The Therapeutic Potential of Nanobodies. *BioDrugs* **2020**, *34*, 11–26. [[CrossRef](#)] [[PubMed](#)]
137. Steeland, S.; Vandenbroucke, R.E.; Libert, C. Nanobodies as therapeutics: Big opportunities for small antibodies. *Drug Discov. Today* **2016**, *21*, 1076–1113. [[CrossRef](#)]
138. Jovčevska, I.; Zupanec, N.; Kočevar, N.; Cesselli, D.; Podergajs, N.; Stokin, C.L.; Myers, M.P.; Muyldermans, S.; Ghassabeh, G.H.; Motaln, H.; et al. TRIM28 and β -actin identified via nanobody-based reverse proteomics approach as possible human glioblastoma biomarkers. *PLoS ONE* **2014**, *9*, e113688. [[CrossRef](#)]
139. Jovčevska, I.; Zupanec, N.; Urlep, Ž.; Vranic, A.; Matos, B.; Stokin, C.L.; Muyldermans, S.; Myers, M.P.; Buzdin, A.A.; Petrov, I.; et al. Differentially expressed proteins in glioblastoma multiforme identified with a nanobody-based anti-proteome approach and confirmed by OncoFinder as possible tumor-class predictive biomarker candidates. *Oncotarget* **2017**, *8*, 44141–44158. [[CrossRef](#)] [[PubMed](#)]
140. Van De Water, J.A.J.M.; Bagci-Onder, T.; Agarwal, A.S.; Wakimoto, H.; Roovers, R.C.; Zhu, Y.; Kasmieh, R.; Bhere, D.; Van Bergen En Henegouwen, P.M.P.; Shah, K. Therapeutic stem cells expressing variants of EGFR-specific nanobodies have antitumor effects. *Proc. Natl. Acad. Sci. USA* **2012**, *109*, 16642–16647. [[CrossRef](#)]
141. Samec, N.; Jovčevska, I.; Stojan, J.; Zottel, A.; Liovic, M.; Myers, M.P.; Muyldermans, S.; Šribar, J.; Križaj, I.; Komel, R. Glioblastoma-specific anti-TUFM nanobody for in-vitro immunoimaging and cancer stem cell targeting. *Oncotarget* **2018**, *9*, 17282–17299. [[CrossRef](#)]
142. Zottel, A.; Jovčevska, I.; Šamec, N.; Mlakar, J.; Šribar, J.; Križaj, I.; Skoblar Vidmar, M.; Komel, R. Anti-vimentin, anti-TUFM, anti-NAP1L1 and anti-DPYSL2 nanobodies display cytotoxic effect and reduce glioblastoma cell migration. *Ther. Adv. Med. Oncol.* **2020**, *12*. [[CrossRef](#)] [[PubMed](#)]
143. Ruiz-López, E.; Schuhmacher, A.J. Transportation of Single-Domain Antibodies through the Blood-Brain Barrier. *Biomolecules* **2021**, *11*, 1131. [[CrossRef](#)]
144. Gao, Y.; Zhu, J.; Lu, H. Single domain antibody-based vectors in the delivery of biologics across the blood-brain barrier: A review. *Drug Deliv. Transl. Res.* **2020**, *11*, 1818–1828. [[CrossRef](#)] [[PubMed](#)]
145. Pothin, E.; Lesuisse, D.; Lafaye, P. Brain delivery of single-domain antibodies: A focus on VHH and VNAR. *Pharmaceutics* **2020**, *12*, 937. [[CrossRef](#)]
146. Bélanger, K.; Iqbal, U.; Tanha, J.; MacKenzie, R.; Moreno, M.; Stanimirovic, D. Single-Domain Antibodies as Therapeutic and Imaging Agents for the Treatment of CNS Diseases. *Antibodies* **2019**, *8*, 27. [[CrossRef](#)]
147. Fishman, J.B.; Rubin, J.B.; Handrahan, J.V.; Connor, J.R.; Fine, R.E. Receptor-mediated transcytosis of transferrin across the blood-brain barrier. *J. Neurosci. Res.* **1987**, *18*, 299–304. [[CrossRef](#)]
148. Fillebeen, C.; Descamps, L.; Dehouck, M.P.; Fenart, L.; Benaïssa, M.; Spik, G.; Cecchelli, R.; Pierce, A. Receptor-mediated transcytosis of lactoferrin through the blood-brain barrier. *J. Biol. Chem.* **1999**, *274*, 7011–7017. [[CrossRef](#)]
149. Muruganandam, A.; Tanha, J.; Narang, S.; Stanimirovic, D. Selection of phage-displayed llama single-domain antibodies that transmigrate across human blood-brain barrier endothelium. *FASEB J.* **2002**, *16*, 240–242. [[CrossRef](#)] [[PubMed](#)]
150. Abulrob, A.; Sprong, H.; Van Bergen En Henegouwen, P.; Stanimirovic, D. The blood-brain barrier transmigrating single domain antibody: Mechanisms of transport and antigenic epitopes in human brain endothelial cells. *J. Neurochem.* **2005**, *95*, 1201–1214. [[CrossRef](#)]
151. Farrington, G.K.; Caram-Salas, N.; Haqqani, A.S.; Brunette, E.; Eldredge, J.; Pepinsky, B.; Antognetti, G.; Baumann, E.; Ding, W.; Garber, E.; et al. A novel platform for engineering blood-brain barrier-crossing bispecific biologics. *FASEB J.* **2014**, *28*, 4764–4778. [[CrossRef](#)]
152. Tamai, I.; Sai, Y.; Kobayashi, H.; Kamata, M.; Wakamiya, T.; Tsuji, A. Structure-internalization relationship for adsorptive-mediated endocytosis of basic peptides at the blood-brain barrier. *J. Pharmacol. Exp. Ther.* **1997**, *280*, 410–415.
153. Hervé, F.; Ghinea, N.; Scherrmann, J.M. CNS delivery via adsorptive transcytosis. *AAPS J.* **2008**, *10*, 455–472. [[CrossRef](#)] [[PubMed](#)]
154. Li, T.; Bourgeois, J.P.; Celli, S.; Glacial, F.; Le Sourd, A.M.; Mecheri, S.; Weksler, B.; Romero, I.; Couraud, P.O.; Rougeon, F.; et al. Cell-penetrating anti-GFAP VHH and corresponding fluorescent fusion protein VHH-GFP spontaneously cross the blood-brain barrier and specifically recognize astrocytes: Application to brain imaging. *FASEB J.* **2012**, *26*, 3969–3979. [[CrossRef](#)]
155. Li, T.; Vandesquille, M.; Koukoulis, F.; Duffeant, C.; Youssef, I.; Lenormand, P.; Ganneau, C.; Maskos, U.; Czech, C.; Gruening, F.; et al. Camelid single-domain antibodies: A versatile tool for in vivo imaging of extracellular and intracellular brain targets. *J. Control. Release* **2016**, *243*, 1–10. [[CrossRef](#)] [[PubMed](#)]
156. Rotman, M.; Welling, M.M.; Bunschoten, A.; De Backer, M.E.; Rip, J.; Nabuurs, R.J.A.; Gaillard, P.J.; Van Buchem, M.A.; Van Der Maarel, S.M.; Van Der Weerd, L. Enhanced glutathione PEGylated liposomal brain delivery of an anti-amyloid single domain antibody fragment in a mouse model for Alzheimer's disease. *J. Control. Release* **2015**, *203*, 40–50. [[CrossRef](#)] [[PubMed](#)]
157. van Lith, S.A.M.; van den Brand, D.; Wallbrecher, R.; van Duijnhoven, S.M.J.; Brock, R.; Leenders, W.P.J. A Conjugate of an Anti-Epidermal Growth Factor Receptor (EGFR) VHH and a Cell-Penetrating Peptide Drives Receptor Internalization and Blocks EGFR Activation. *ChemBioChem* **2017**, *18*, 2390–2394. [[CrossRef](#)]
158. Yin, W.; Zhao, Y.; Kang, X.; Zhao, P.; Fu, X.; Mo, X.; Wan, Y.; Huang, Y. BBB-penetrating codelivery liposomes treat brain metastasis of non-small cell lung cancer with EGFR790M mutation. *Theranostics* **2020**, *10*, 6122–6135. [[CrossRef](#)]

159. Chakravarty, R.; Goel, S.; Cai, W. Nanobody: The “magic bullet” for molecular imaging? *Theranostics* **2014**, *4*, 386–398. [[CrossRef](#)]
160. Iqbal, U.; Trojahn, U.; Albaghdadi, H.; Zhang, J.; O’Connor-Mccourt, M.; Stanimirovic, D.; Tomanek, B.; Sutherland, G.; Abulrob, A. Kinetic analysis of novel mono- and multivalent VHH-fragments and their application for molecular imaging of brain tumours: RESEARCH PAPER. *Br. J. Pharmacol.* **2010**, *160*, 1016–1028. [[CrossRef](#)]
161. Fatehi, D.; Baral, T.N.; Abulrob, A. In vivo imaging of brain cancer using epidermal growth factor single domain antibody bioconjugated to near-infrared quantum dots. *J. Nanosci. Nanotechnol.* **2014**, *14*, 5355–5362. [[CrossRef](#)]
162. Iqbal, U.; Albaghdadi, H.; Luo, Y.; Arbabi, M.; Desvaux, C.; Veres, T.; Stanimirovic, D.; Abulrob, A. Molecular imaging of glioblastoma multiforme using anti-insulin-like growth factor-binding protein-7 single-domain antibodies. *Br. J. Cancer* **2010**, *103*, 1606–1616. [[CrossRef](#)]
163. Iqbal, U.; Albaghdadi, H.; Nieh, M.P.; Tuor, U.I.; Mester, Z.; Stanimirovic, D.; Katsaras, J.; Abulrob, A. Small unilamellar vesicles: A platform technology for molecular imaging of brain tumors. *Nanotechnology* **2011**, *22*, 195102. [[CrossRef](#)]
164. Vosjan, M.J.W.D.; Vercammen, J.; Kolkman, J.A.; Stigter-Van Walsum, M.; Revets, H.; Van Dongen, G.A.M.S. Nanobodies targeting the hepatocyte growth factor: Potential new drugs for molecular cancer therapy. *Mol. Cancer Ther.* **2012**, *11*, 1017–1025. [[CrossRef](#)] [[PubMed](#)]
165. Vandesquille, M.; Li, T.; Po, C.; Ganneau, C.; Lenormand, P.; Duffeffant, C.; Czech, C.; Grueninger, F.; Duyckaerts, C.; Delatour, B.; et al. Chemically-defined camelid antibody bioconjugate for the magnetic resonance imaging of Alzheimer’s disease. *mAbs* **2017**, *9*, 1016–1027. [[CrossRef](#)] [[PubMed](#)]
166. Rotman, M.; Welling, M.M.; van den Boogaard, M.L.; Moursel, L.G.; van der Graaf, L.M.; van Buchem, M.A.; van der Maarel, S.M.; van der Weerd, L. Fusion of hIgG1-Fc to 111In-anti-amyloid single domain antibody fragment VHH-pa2H prolongs blood residential time in APP/PS1 mice but does not increase brain uptake. *Nucl. Med. Biol.* **2015**, *42*, 695–702. [[CrossRef](#)] [[PubMed](#)]
167. Debie, P.; Devoogdt, N.; Hernot, S. Targeted Nanobody-Based Molecular Tracers for Nuclear Imaging and Image-Guided Surgery. *Antibodies* **2019**, *8*, 12. [[CrossRef](#)] [[PubMed](#)]
168. Duggan, S. Caplacizumab: First Global Approval. *Drugs* **2018**, *78*, 1639–1642. [[CrossRef](#)]
169. Scully, M.; Cataland, S.R.; Peyvandi, F.; Coppo, P.; Knöbl, P.; Kremer Hovinga, J.A.; Metjian, A.; de la Rubia, J.; Pavenski, K.; Callewaert, F.; et al. Caplacizumab Treatment for Acquired Thrombotic Thrombocytopenic Purpura. *N. Engl. J. Med.* **2019**, *380*, 335–346. [[CrossRef](#)]
170. Keyaerts, M.; Xavier, C.; Heemskerk, J.; Devoogdt, N.; Everaert, H.; Ackaert, C.; Vanhoeij, M.; Duhoux, F.P.; Gevaert, T.; Simon, P.; et al. Phase I study of 68Ga-HER2-Nanobody for PET/CT assessment of HER2 expression in breast carcinoma. *J. Nucl. Med.* **2016**, *57*, 27–33. [[CrossRef](#)]
171. Xing, Y.; Chand, G.; Liu, C.; Cook, G.J.R.; O’Doherty, J.; Zhao, L.; Wong, N.C.L.; Meszaros, L.K.; Ting, H.H.; Zhao, J. Early phase I study of a 99mTc-labeled anti-programmed death ligand-1 (PD-L1) single-domain antibody in SPECT/CT assessment of PD-L1 expression in non-small cell lung cancer. *J. Nucl. Med.* **2019**, *60*, 1213–1220. [[CrossRef](#)]
172. Sinigaglia, M.; Assi, T.; Besson, F.L.; Ammari, S.; Edjlali, M.; Feltus, W.; Rozenblum-Beddok, L.; Zhao, B.; Schwartz, L.H.; Mokrane, F.Z.; et al. Imaging-guided precision medicine in glioblastoma patients treated with immune checkpoint modulators: Research trend and future directions in the field of imaging biomarkers and artificial intelligence. *EJNMMI Res.* **2019**, *9*, 78. [[CrossRef](#)]
173. Escudero, L.; Martinez-Ricarte, F.; Seoane, J. ctDNA-Based Liquid Biopsy of Cerebrospinal Fluid in Brain Cancer. *Cancers* **2021**, *13*, 1989. [[CrossRef](#)]
174. Diaz, L.A., Jr.; Bardelli, A. Liquid Biopsies: Genotyping Circulating Tumor DNA. *J. Clin. Oncol.* **2014**, *32*, 579–586. [[CrossRef](#)]
175. Siravegna, G.; Mussolin, B.; Venesio, T.; Marsoni, S.; Seoane, J.; Dive, C.; Papadopoulos, N. How liquid biopsies can change clinical practice in oncology. *Ann. Oncol.* **2019**, *30*, 1580–1590. [[CrossRef](#)]
176. Bettgowda, C.; Sausen, M.; Leary, R.J.; Kinde, I.; Wang, Y.; Agrawal, N.; Bartlett, B.R.; Wang, H.; Luber, B.; Alani, R.M.; et al. Detection of Circulating Tumor DNA in Early- and Late-Stage Human Malignancies. *Sci. Transl. Med.* **2014**, *6*, 250ra115. [[CrossRef](#)] [[PubMed](#)]
177. De Mattos-Arruda, L.; Mayor, R.; Ng, C.K.Y.; Weigelt, B.; Marti, F.; Torrejon, D.; Oliveira, M.; Arias, A.; Raventos, C.; Tang, J.; et al. Cerebrospinal fluid-derived circulating tumour DNA better represents the genomic alterations of brain tumours than plasma. *Nat. Commun.* **2015**, *6*, 8839. [[CrossRef](#)] [[PubMed](#)]
178. Wei, W.; Rosenkrans, Z.T.; Liu, J.; Huang, G.; Luo, Q.; Cai, W. ImmunopET: Concept, Design, and Applications. *Chem. Rev.* **2020**, *120*, 3787–3851. [[CrossRef](#)] [[PubMed](#)]
179. Dewulf, J.; Adhikari, K.; Vangestel, C.; Wyngaert, T. Van Den Development of Antibody Immuno-PET / SPECT Radiopharmaceuticals for Imaging of Oncological. *Cancers* **2020**, *12*, 1868. [[CrossRef](#)] [[PubMed](#)]
180. Bolcaen, J.; Kleyhans, J.; Nair, S.; Verhoeven, J.; Goethals, I.; Sathegke, M.; Vandevoorde, C.; Ebenhan, T. A perspective on the radiopharmaceutical requirements for imaging and therapy of glioblastoma. *Theranostics* **2021**, *11*, 7911–7947. [[CrossRef](#)]
181. Langbein, T.; Weber, W.A.; Eiber, M. Future of theranostics: An outlook on precision oncology in nuclear medicine. *J. Nucl. Med.* **2019**, *60*, 13S–19S. [[CrossRef](#)] [[PubMed](#)]
182. Li, D.; Patel, C.B.; Xu, G.; Iagaru, A.; Zhu, Z.; Zhang, L.; Cheng, Z. Visualization of Diagnostic and Therapeutic Targets in Glioma With Molecular Imaging. *Front. Immunol.* **2020**, *11*, 592389. [[CrossRef](#)]
183. Sarkaria, J.N.; Hu, L.S.; Parney, I.F.; Pafundi, D.H.; Brinkmann, D.H.; Laack, N.N.; Giannini, C.; Burns, T.C.; Kizilbash, S.H.; Laramy, J.K.; et al. Is the blood-brain barrier really disrupted in all glioblastomas? A critical assessment of existing clinical data. *Neuro-Oncology* **2018**, *20*, 184–191. [[CrossRef](#)] [[PubMed](#)]

184. Caljon, G.; Stijlemans, B.; Saerens, D.; van den Abbeele, J.; Muyltermans, S.; Magez, S.; de Baetselier, P. Affinity Is an Important Determinant of the Anti-Trypanosome Activity of Nanobodies. *PLoS Negl. Trop. Dis.* **2012**, *6*, e1902. [[CrossRef](#)]
185. Ackaert, C.; Smiejkowska, N.; Xavier, C.; Sterckx, Y.G.J.; Denies, S.; Stijlemans, B.; Elkrim, Y.; Devoogdt, N.; Caveliers, V.; Lahoutte, T.; et al. Immunogenicity Risk Profile of Nanobodies. *Front. Immunol.* **2021**, *12*, 578. [[CrossRef](#)] [[PubMed](#)]
186. Vejt, E.; De Jong, M.; Wetzels, J.F.M.; Masereeuw, R.; Melis, M.; Oyen, W.J.G.; Gotthardt, M.; Boerman, O.C. Renal Toxicity of Radiolabeled Peptides and Antibody Fragments: Mechanisms, Impact on Radionuclide Therapy, and Strategies for Prevention. *J. Nucl. Med.* **2010**, *51*, 1049–1058. [[CrossRef](#)] [[PubMed](#)]
187. Wang, C.; Chen, Y.; Hou, Y.N.; Liu, Q.; Zhang, D.; Zhao, H.; Zhang, Y.; An, S.; Li, L.; Hou, J.; et al. ImmunoPET imaging of multiple myeloma with [68Ga]Ga-NOTA-Nb1053. *Eur. J. Nucl. Med. Mol. Imaging* **2021**, *48*, 2749–2760. [[CrossRef](#)]
188. Rashidian, M.; LaFleur, M.W.; Verschoor, V.L.; Dongre, A.; Zhang, Y.; Nguyen, T.H.; Kolifrath, S.; Aref, A.R.; Lau, C.J.; Paweletz, C.P.; et al. Immuno-PET identifies the myeloid compartment as a key contributor to the outcome of the antitumor response under PD-1 blockade. *Proc. Natl. Acad. Sci. USA* **2019**, *116*, 16971–16980. [[CrossRef](#)]
189. Rashidian, M.; Ingram, J.R.; Dougan, M.; Dongre, A.; Whang, K.A.; LeGall, C.; Cragolini, J.J.; Bieri, B.; Gostissa, M.; Gorman, J.; et al. Predicting the response to CTLA-4 blockade by longitudinal noninvasive monitoring of CD8 T cells. *J. Exp. Med.* **2017**, *214*, 2243–2255. [[CrossRef](#)]
190. Xavier, C.; Vaneycken, I.; D’huyvetter, M.; Heemskerk, J.; Keyaerts, M.; Vincke, C.; Devoogdt, N.; Muyltermans, S.; Lahoutte, T.; Caveliers, V. Synthesis, Preclinical Validation, Dosimetry, and Toxicity of 68 Ga-NOTA-Anti-HER2 Nanobodies for iPET Imaging of HER2 Receptor Expression in Cancer. *J. Nucl. Med.* **2013**, *54*, 776–784. [[CrossRef](#)] [[PubMed](#)]
191. Bridoux, J.; Broos, K.; Lecocq, Q.; Debie, P.; Martin, C.; Ballet, S.; Raes, G.; Neyt, S.; Vanhove, C.; Breckpot, K.; et al. Anti-Human PD-L1 Nanobody for Immuno-PET Imaging: Validation of a Conjugation Strategy for Clinical Translation. *Biomolecules* **2020**, *10*, 1388. [[CrossRef](#)]
192. Chigoho, D.M.; Lecocq, Q.; Awad, R.M.; Breckpot, K.; Devoogdt, N.; Keyaerts, M.; Caveliers, V.; Xavier, C.; Bridoux, J. Site-Specific Radiolabeling of a Human PD-L1 Nanobody via Maleimide–Cysteine Chemistry. *Pharmaceuticals* **2021**, *14*, 550. [[CrossRef](#)] [[PubMed](#)]